PQ²

A Brighter Future Without Flickering Lights
Designing a Low Cost Power Quality Analyzer

EE3L11: Bachelor Graduation Project Electrical Engineering

Eline Bouma, Luke Damoiseaux
& Jorik Groeneveld

Delft University of Technology

TU Delft

A Brighter Future Without Flickering Lights
Designing a Low Cost Power Quality Analyzer

by

Eline Bouma, Luke Damoiseaux & Jorik Groeneveld

Student Name	Student Number
Eline Bouma	5321719
Luke Damoiseaux	5263700
Jorik Groeneveld	5137683

Internal proposer and group supervisor:	Simona Renzaglia
Project supervisors:	Prof. Dr. Peter Palensky & Dr. Aleksandra Lekić
Practical supervisor:	Ing. Remko Koornneef
Project Duration:	September, 2023 - January, 2024
Faculty:	Faculty Electrical Engineering, Mathematics and Computer Science Delft

Cover: Computer generated render of Power Quality Analyzer Using Fusion 360

TU Delft

Preface

This thesis is part of the Electrical Engineering Bachelor's graduation project at TU Delft. The goal of the thesis is to design a power quality analyzer. Although we are finishing our bachelor's soon, when receiving the proposal for this thesis we realized we had never truly considered power quality and the potential challenges it poses. It reminded us just how vast the world of electrical engineering is. Throughout this project, we learned just how significant power quality is and the influence power electronics have on it. Designing a device to detect these issues was challenging, but it was also a fulfilling task with a direct relation to an emerging problem in the energy sector.

We extend special thanks to our supervisors; Dr. Aleksandra Lekić whose agenda was always full, yet she still always found time for us, Ing. Remko Koornneef whose laugh (and really cool lab) never failed to make us (Luke) smile, and Ms. Simona Renzaglia, who might have learned more about electrical engineering than she would have liked. Your guidance and support were instrumental in navigating the complexities of this project.

Special thanks are also extended to the staff of the Tellegen Hall, Ing. Martin Schumacher, and Ing A.M.J "Ton" Slats, for providing practical assistance, fun conversations, and always opening locked doors, often multiple times a day. Our gratitude also extends to Dr. Ing. Ioan E. Lager for granting us the opportunity to undertake this thesis and for consistently providing support whenever we sought guidance.

Finally, a special thanks to Emirhan Öztürkoglu, Marten de Vries, and Hüsna Yıldız of the software team. It was a pleasure working with you all on this project.

Eline Bouma, Luke Damoiseaux
& Jorik Groeneveld
Delft, January 2024

Abstract

The increase in non-linear loads of modern electronics raises concerns over power quality. Additionally, existing power-quality analyzers are expensive and not intended for household use. This thesis aims to develop a single-phase, user-friendly power-quality analyzer using a Raspberry Pi 4 Model B with an emphasis on low cost and class S specifications. The design was split into modules consisting of analog to digital conversion, voltage sensing, and current sensing. Sub-modules were added for circuit protection and PCB. Various approaches are discussed before circuit design, simulation, and testing occur. A functioning prototype was assembled on a dedicated PCB while not exceeding the set budget of €250.00. However, it could not be determined whether the class S specifications were achieved due to insufficient testing. A variety of improvements have been suggested.

Contents

Nomenclature

In this report some abbreviations are used, these are stated in the Table 1 below.

Abbreviations

Abbreviation	Definition
AC	Alternating Current
ADC	Analog Digital Converter
AMR	Anisotropic Magneto Resistance
CMC	Common Mode Choke
DC	Direct Current
GMR	Giant Magneto Resistance
GPIO	General Purpose Input/Output
IEC	International Electrotechnical Commission
IEEE	Institute of Electrical and Electronics Engineers
IIR	Infinite Impulse Response
I2C	Inter-Integrated Circuit
LSB	Least Significant Bit
MFB	Multiple Feedback
Op amp	Operational Amplifier
PCB	Printed Circuit Board
Pk-Pk	Peak To Peak
RLC	Resistive Inductive Capacitive
RMS	Root Mean Square
PoR	Program of requirements
SAR	Successive Approximation
SMD	Surface Mounted Device
SPI	Serial Peripheral Interface
THT	Through Hole Technology
ToR	Trade off requirements
TVS	Transient Voltage Suppression

1

Introduction

Power quality, as defined by the Institute of Electrical and Electronics Engineers (IEEE), is *"the concept of powering and grounding sensitive electronic equipment in a manner that is suitable to the operation of that equipment."*[1]. Consequently, power quality analysis is the process in which relevant factors are measured and analyzed to determine their compliance with set international safety and quality standards. As a result, deviation level thresholds are set in place by the European Union as stated in the EN 50160 document to ensure that power delivered by the energy supplier is reliable and of acceptable power quality [2].

Disturbances to power quality can be classified as different events. These disturbances include transient voltage spikes, over-voltage, voltage swells/surges and voltage dips/sags, frequency fluctuations, flicker, interruptions, harmonic distortions, and low power factor [3]. The focus of this thesis is the detection of some or all of these events, and thus the causes of these disturbances go beyond the scope of this thesis. Power quality analysis is important as these disturbances to power quality can result in damage to electronics, data corruption, flickering lights, increased energy consumption, discomfort, and potential safety concerns [4]. The impact of poor power quality is not just limited to a small subset of businesses, but rather a large variety of consumers, including households. According to a 2004-2005 power quality survey [5], domestic customers account for 56% of power quality complaints in the Netherlands while commercial, agricultural, and industrial customers account for 12%, 11%, and 10% respectively. Additionally, customers cause 70% of power quality disturbances in the USA, and therefore unsurprisingly, network operators refuse to take full responsibility for said issues [6]. It is important to note that power delivery methods influence the types of power quality disturbances that occur. Voltage dips and transients are more prevalent in countries where overhead lines are used due to natural occurrences such as lighting strikes while countries with underground cables encounter more issues with harmonics and resonance [4].

Power quality is an area of growing concern. The introduction of power electronics is causing high-frequency harmonics between the 2 kHz and 150 kHz range which could result in many issues in the future if not addressed properly [7]. This is especially relevant today as a large amount of emphasis is placed on the transition to renewable energy systems where power electronics play a significant role [8], hence these high-frequency harmonics will only become more prevalent. Additionally, the cause of these harmonics is not only limited to the renewable energy sector. Non-linear loads in modern electronics are everywhere in households. LED lights, induction stoves, and electric vehicles are just some examples of modern electronics that use non-linear loads. Modern society is heavily dependent on these devices and unfortunately, they also negatively impact power quality [9].

Power quality analyzers are devices designed to record data on power quality distortions and identify issues related to the power quality. Currently, power quality analyzers appear to be marketed towards large firms. This observation is reflected by their high price, generally three-phase system functionality [10], and lack of simple user installation and interface. This makes these devices unsuitable for households, small businesses, or even educational uses. This project aims to design a power-quality

analyzer at a low cost that operates on single-phase systems and is user-friendly. This thesis will focus on the hardware design required for this to be achieved.

1.1. State of the art analysis

It is important to address the fact that power quality analyzers are not a new concept as seen by the hundreds of different models available for purchase, although few of these are designed for single-phase systems and even fewer are low-cost. There is an already existing demand for power quality analyzers which is expected to grow further as a result of increased growth of renewable energy and concern over grid power quality [10].

This is also not the first attempt at designing such a power quality analyzer and there is already a considerable amount of studies that have attempted to design something similar. However, this is advantageous as information from these studies can be used as a starting point for the development of the device. For instance, the research openZmeter [11] employs an ARM Linux board and an STM32 microcontroller while another research study [12] uses and ESP32 and yet another study [13] also uses an ESP32 but with an MCP3008 ADC. Other studies [14] have also been found that use a Raspberry Pi Model B+ but does not measure current or another which uses a Raspberry Pi Zero W microcontroller [15]. Five potential options for the ADC have already been mentioned and each could be discussed further to determine which would be best. A similar approach to this is done for each module individually during the design process.

1.2. Thesis Structure

This thesis is organized as follows. Chapter 2 contains the programme of requirements for the entire system and the hardware group which is used to guide the development process. Chapter 3 contains the division of the design into the major modules. The following Chapters (4, 5, 6) thoroughly discuss the design process of these major modules and generally follow the structure of discussing preliminary research, component selection, simulation, and testing. Chapter 7 discusses steps taken to ensure safe working practices as well as the circuit protection implemented into the design. Afterwards, the results of measurements made using the entire system are presented and discussed in Chapter 8. This is followed by a discussion in Chapter 9 evaluating the performance of the prototype compared to the requirements and future improvements that could be made. Finally, a conclusion can be found in Chapter 10.

2

Programme of Requirements

2.1. Requirements for the entire system

The goal of this Bachelor's graduation project is to build a low cost solution to measure power quality. The device should be able to detect distortions and harmonics in the grid. The device should be an embedded device with a single-board computer suitable for use with mains electricity. The consumer should be able to review real-time data and access stored data of power quality irregularities to get an idea about the power quality in their house. This product will help the user gain insight into their power quality. The product does not solve the issues, it simply collects data on the occurrence of these issues and provides this for the consumer to review.

The system must:

- S.1 Be able to record voltage waveform independent of power consumption
- S.2 Present real-time waveform data
- S.3 Be able to measure the power consumption of any device that falls within the set limitations
- S.4 Designed in separate modules
- S.5 Implement a Raspberry Pi 4 Model B
- S.6 Be able to store a full month's worth of data
- S.7 Meet the specifications of a Class S power quality analyzer (Table 2.1)
- S.8 Costs less than €250 to assemble

2.2. Requirements for the hardware subgroup

This thesis is divided into two subgroups. This subgroup will design the hardware that is responsible for everything from the power socket up to the Raspberry Pi. The goal of this subgroup is to transform high voltage and high current signals from the grid into the digital domain. After this point, the software subgroup is responsible for data processing and interface using a Raspberry Pi. The following requirements are specific to the hardware subgroup.

The subsystem must:

1. Device layout
   - 1.1 Provide power from the grid using one type F socket to power both the device itself and a possible connected load.
   - 1.2 Contain a type F socket for a load to be connected in series with the device
2. Device functionality

2.1 Be capable of voltage and current waveform detection

2.2 Voltage and current detection work independently of each other

2.3 Work on single phase systems operating at 230V RMS at 50 Hz

3. Specific requirements

3.1 Meet class S requirements set by IEC 61000-4-30 (Table 2.1)

3.2 Meet class S accuracy requirements set by IEC 61000-4-7 (Table 2.2)

3.3 Operate over a bandwidth of 10 Hz to 10 kHz such that up to the 200th harmonic could be detected if desired

3.4 Be able to operate in a system with a Class B 1 Pole Breaker of 16A [16]

4. Safety requirements

4.1 An enclosure must be designed for the device

4.2 Device must be galvanically isolated from mains

4.3 Device must include overvoltage, overcurrent and thermal protection

5. ADC Requirements:

5.1 At least 10-bit resolution

5.2 At least 12.8 kSps sampling rate (256 samples per period) per channel [17]

5.3 ADC must be compatible with I2C or SPI

5.4 The ADC must either have a sufficient number of channels for the required signals or be capable of address selection if multiple ADCs are used

Table 2.1: Class S requirements according to IEC-61000-4-30 [18]

Parameter	Uncertainty	Measuring range
Frequency	$\pm$50 mHz	42.5 Hz to 57.5 Hz
Magnitude of the supply	$\pm$ 0.5 % U_{din}	20 % to 120 % U_{din}
Dips and swells	Amplitude $\pm$1% U_{din} Duration $\pm$1 cycle or $\pm$2 cycles	N/A
Unbalance	$\pm$0.3%	1% to 5% of u_2 (if implemented same for u_0)
Voltage harmonics	200% of IEC 61000-4-7 Class 2	10% to 100% of Class 3 of IEC61000-2-4
Current	$\pm$2%	10% FS to 100% FS

Table 2.2: Accuracy Standards according to IEC-61000-4-7 [19]

Class	Measurement	Conditions	Maximum Error
A	Voltage	U_M ≥ 1% U_{NOM} U_M <1% U_{NOM}	±5% U_M ±0.05% U_{NOM}
	Current	I_M ≥ 3% I_{NOM} I_M <3% I_{NOM}	±5% I_M ±0.15% I_{NOM}
	Power	P_M ≥ 150 W P_M <150 W	±1% P_M ±1.5% W
S	Voltage	U_M ≥ 3% U_{NOM} U_M <3% U_{NOM}	±5% U_M ±0.15% U_{NOM}
	Current	I_M ≥ 10% I_{NOM} I_M <10% I_{NOM}	±5% I_M ±0.5% I_{NOM}

2.3. Trade Off Requirements

The following requirements are not necessary for a functional prototype, however, they would further increase the capabilities of the device. These requirements also act as a future road map if they are not realized within the span of this project.

ToR.1 Design a dedicated PCB for the device

ToR.2 Implement an uninterruptible power supply (UPS) such that the device continues operation during power disruptions

ToR.3 Implement a transient detection system

ToR.4 Ability to operate on and measure DC

3

Design overview

Figure 3.1 depicts the initial design idea of the device before circuit design began such that all members were in agreeance over the functionality of the device. The general concept is that the device would have only one plug and be a closed box having only a socket for a load to be connected for current measurements and access to a USB port to physically access data measurements. The group was divided into two teams: a hardware subgroup and a software subgroup.

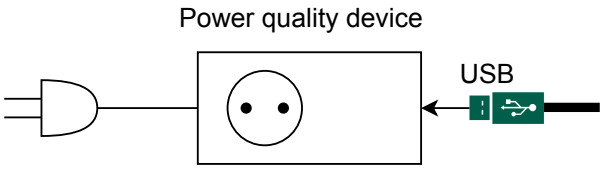

Figure 3.1: Initial Design Overview

3.1. Modules

The design process of the Hardware group was divided into 3 main modules required for the device to operate which can be seen in Figure 3.2, which are: ADC, voltage sensing, current sensing. The general approach for each module was to start by reviewing the approach other studies had taken, simulating and testing components, designing filters if needed, and then testing the individual modules before integrating them. Additional sub-modules for safety, circuit protection, and PCB design were added at a later stage. The software group was responsible for managing the Raspberry Pi and handling the data processing tasks.

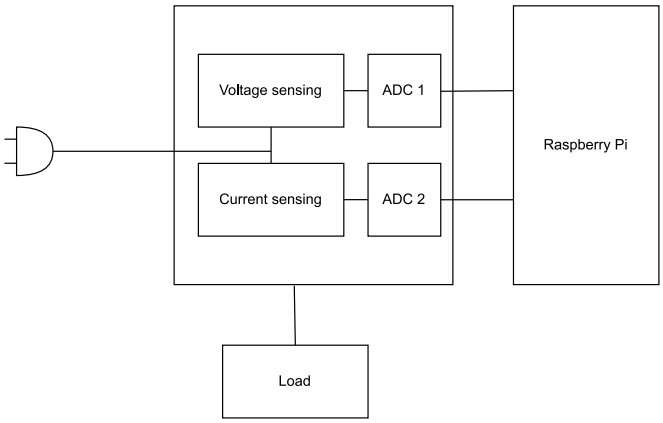

Figure 3.2: Block diagram of the design modules

4

Analog-to-Digital Conversion

The purpose of the analog-to-digital conversion module is to convert the analog signals provided by the voltage and current sensors into a digital value to be communicated to the Raspberry Pi. Requirements 5.1 to 5.4 are used to guide the ADC selection. In this chapter, research into what other studies have done will be discussed first, followed by a description of the selected ADC and a justification as to why.

4.1. Preliminary Research

Many different ADCs could be used for the analog-to-digital conversion section. For example, the openzmeter (oZm) is an open-source system that uses the STM32 microcontroller with a built-in 12-bit SAR ADC and an embedded ARM unit for its processing [11]. In another study [12], the ESP32 microcontroller, also with a built-in 12-bit SAR ADC is used. However, it was decided that using a separate microcontroller with an ADC would add a level of complexity regarding communication with the Raspberry Pi for an ADC which could be avoided, therefore both of these approaches would not be applicable. A potential ADC used in another research study was the MCP3008 [13]. However, this ADC has a 10-bit resolution which when considering error, might not suffice with our minimum 10-bit resolution. Another ADC that was found independently and considered was the EVAL-AD7988-1-PMDZ. Although this ADC has a higher resolution, it only has a single channel and would require more than one to be implemented. Using an additional ADC is not an issue on its own, but an ADC with more channels allows for more flexibility in the design. Lastly, another ADC is the ADE9000 which is a dedicated chip meant for power quality applications. It even has built-in digital signal processing to calculate factors such as apparent power, power factor voltage swells, etc. However, using a dedicated chip like this would reduce the flexibility of the design and signal processing as well as create issues if the chip is no longer produced as it would not be simple to replace. Additionally, this ADC would require a dedicated PCB to be designed before testing could be done.

4.2. Chosen ADC

The ADC found to be suitable for this project is the AD7142-Q1, a 12-bit successive approximation register (SAR) developed by Texas Instruments. All of the subsequent information regarding the specifications of the AD7142-Q1 was obtained from the datasheet provided by Texas Instruments [20]. A block diagram of the AD7142-Q1 can be found in Figure A.1.

This ADC was selected for multiple reasons. The first of which is that there is an existing breakout board, the ADC 16 CLICK, produced by MIKROE using this ADC. The advantage of this is that it reduces the development time required before testing as a PCB does not need to be produced in the early stages of design. This also allows for communication between the ADC and Raspberry Pi to be implemented at an earlier stage of development. Another advantage of this ADC is the supply voltage can be powered directly through the GPIO pins of the Raspberry Pi which operates at 3.3V further simplifying the circuit design. Additionally, the ADC is I2C compatible (Requirement 5.3) as well as

having I2C address selection in the case that multiple ADCs are used (Requirement 5.4).

According to the datasheet, the ADC can achieve a maximum sampling rate of 140kSps which would be 2800 samples per period of a 50Hz sinusoidal signal. In the case of the ADC operating in dual channel configuration, the sampling rate of each channel is halved due to the multiplexer (only one channel can be sampled at a time and samples are taken sequentially) which can be seen in Figure A.1. This would result in a sampling rate of 70kSps per channel, which would be 1400 samples per period. Therefore, this would exceed the requirements set (Requirement 5.2).

The ADC also has a 12-bit resolution which fulfills Requirement 5.1. Note that even when accounting for the maximum gain and offset error, the effective resolution of the ADC is above 11.9 bits. This ADC also has a high precision mode that can effectively obtain a resolution of 16-bit by accumulating 16 12-bit conversion results. This would significantly improve the performance of the ADC. However, a major issue is that this would also reduce the sampling rate to a sixteenth of the original sampling rate. For single-channel operation this would be 175 samples per period and for dual-channel operation this would be 87.5 samples per period. Therefore high-precision mode would result in an insufficient sampling rate according to Requirement 5.2.

Lastly, this ADC can be configured to have two single-ended channels, one single-ended channel with remote ground sensing, or one pseudo-differential channel. This provides flexibility regarding design changes as it presents the option of using a pseudo-differential or a single-ended channel with remote ground sensing if multiple ADCs are used. A pseudo-differential configuration is advantageous as it cancels small common-mode voltages [21] which could present itself as an issue later.

4.3. ADC Implementation

Figure 4.1 shows how the ADCs are implemented into the circuit. As can be seen, two ADCs are used. One ADC is reserved for the voltage sensing module and is set up with a reference voltage signal such that the ADC could operate in a single channel single-ended or pseudo-differential configuration. Testing can be done at a later stage to determine which configuration is more optimal. In comparison, the other ADC is reserved for the current sensing module and both channels are used thus the ADC will be operating in a dual-channel single-ended configuration. The reason for this will be discussed in Section 6.3.1.

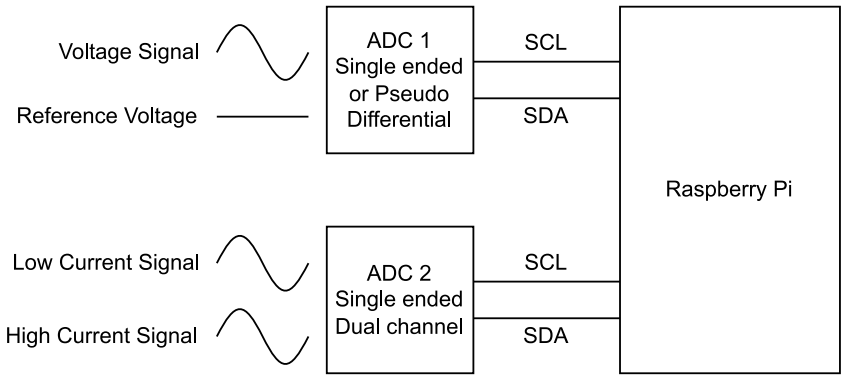

Figure 4.1: ADC connection implementation block diagram

The upper limit of the analog input range is determined by the supply voltage provided while the lower limit is simply 0V. As mentioned previously, the ADCs are powered using the GPIO pins of the Raspberry Pi which provide a voltage of 3.3V. Therefore, the analog input range of the ADC is 0 to 3.3V. This is important throughout the development of the coming modules as they must be designed such that the entire input range is used to maximize the accuracy of the system.

5

Voltage sensing

The goal of the voltage sensor is to convert the voltages from the electricity net into a lower voltage in order for the ADC to make a reading. Achieving this, it is crucial to transmit the frequencies specified in Requirement 3.3. Simultaneously, the higher frequencies that are not within the desired bandwidth should be filtered out. As a safety requirement, Requirement 4.2, the primary side (connected to the grid) and the secondary side (used for measuring) should be isolated from each other preventing the possibility of high voltages existing in comparison to ground on the secondary side. An ideal voltage sensor should have an infinite input impedance, eliminating the current through the source impedance. However the ADC will need to have a minimum current to charge the sample capacitors. This will not be an issue since the electricity grid is able to supply multiple kilowatts of power. A bigger issue is the power dissipation as soon as current is drawn, at $230V_{RMS}$ multiple watts of power can already be consumed with milliamps of current flowing.
In this chapter first, some approaches from literature will be discussed together with their pros and cons. Afterwards, the applied method will be explained and test results using this approach will be shown.

5.1. Different Approaches

To measure the voltage, decisions should be made on what to implement. The initial approach was to use a common mode choke, SBT-0140W. The common mode choke (CMC) was recommended by Analog Devices because it can measure AC line voltage. Furthermore, CMC has the ability to filter the signal by blocking high-frequency noise and letting the desired signal pass through [22].

Common mode choke

The way it was proposed to use the CMC is to first convert the mains voltage to a small current via resistors, then the CMC suppresses the noise by using the inductance on the primary side, then at the output, an operational amplifier is used to convert the current to a voltage. By using this approach, the signal is filtered and the voltage is scaled down [22]. The disadvantage of this method is that the frequency characteristics of the SBT-0140W in the datasheet [23] were rated for a bandwidth starting at 1 MHz till 1000 MHz. Since the bandwidth of the product should be between 10 Hz and 10 kHz, Requirement item 3.3, it was decided not to use this approach.

Resistive network

The research papers: openZmeter [11], Electric power quality analyzer using open-source [14], and the Open Power Quality [15] use a potential divider network. An illustration of a resistor divider network can be seen in Figure 5.1. It has an output voltage over R2 of $V_{out} = V_{in} \cdot \frac{R_2}{R_1+R_2}$. With a total power flow of $P_{in} = V_{in}^2/(R_1 + R_2)$.

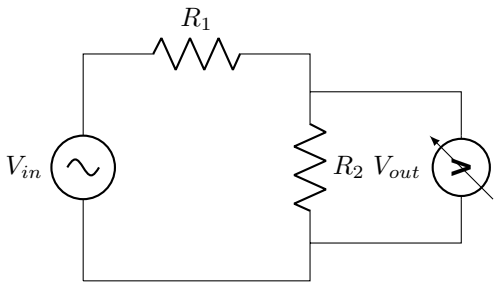

Figure 5.1: Resistor divider

The advantages of using such a resistive network as a voltage sensor is that it is simple to implement and it has a wide range of applications. However, the loading effect on the measured circuit and limited accuracy might create issues [24]. The loading effect is the effect of the load impedance on the source. It happens when a load is connected to the circuit and has an impact on the properties, such as the voltage or current. For resistive loading, which happens in a resistive network, the only impact on the circuit is a voltage drop[25]. The resistors introduce heat dissipation, which might lead to power losses and less accurate measurements. In the worst-case scenario, the heat dissipation might also lead to the resistors overheating. In conjunction with these disadvantages, the resistor divider does not meet Requirement 4.2 of decoupling the AC live wire from the circuit, thus on its own is not sufficient.
However, there are a few solutions to provide galvanic isolation when a resistive network is used. For example, the openZmeter [11] has galvanic isolation for the voltage and current inputs and the ARM board through optocouplers. An optocoupler is a semiconductor device which allows the transmission of signals between two circuits. It provides electrical isolation. It consists of a light emitter, which transmits a light signal, and a light sensor, which detects the signal and converts it to an electrical signal [26] [26]. The advantages of optocouplers are that they can remove noise, they are compact, cheap and have a low power consumption. However, there are also some critical disadvantages of optocouplers. For example, the high-frequency response is poor and they don't have a linear behaviour when the input changes[26]. It is desired to have an as accurate as possible product, which is not affected by changing inputs. Therefore this approach is not used.

Another approach is to use an isolation amplifier, this is used by the researches: the Electric Power Quality Analyzer [14] and the Open Power Quality [15]. An isolation amplifier works like any other amplifier, except that it doesn't have conductive contact between the input and output circuit, proving galvanic isolation. The isolation amplifier consists of an input circuit, isolation barrier and an output circuit. This is a very good solution for the galvanic isolation and if the resistor divider approach would be chosen, this is how it would be done. However, let's first look at different approaches.[14, 15]

Current type voltage tranformer

Another approach is to use a current-type voltage transformer, often found in combination with a dual op amp. This approach was used in the research Development of a smart meter for power quality-based tariff implementation in a smart grid [13]. Common boards use the ZMPT101B tranformer and have an active output. These boards can handle AC input voltages up to 250V(50/60Hz), and the dual op amp provides an output DC voltage up to 5V [27]. The advantage of using this voltage sensor is that it features a transformer, which provides galvanic isolation for the circuit. It claimed to be highly accurate, it has a large input range from 0- 1000V and the operating temperature works for our application as well. However, there are a few issues with this product. First of all, the data sheet did not contain a lot of information, it was not very clear what frequency response would be[28]. Secondly, the voltage sensor is only sold on unreliable web shops, such as Ali Express. For our project it was preferred to use European/Dutch component web shops, because of their reliability. Furthermore, the shipping would take too long from non-European web shops.

Voltage transformer

Instead of using a current-type voltage transformer, a normal voltage transformer could be used.
The voltage transformer is illustrated in Figure 5.2. The voltage transformer will serve two main pur-

poses in this design: decoupling the live AC mains wires from the device, which provides the required isolation, and down-converting the voltage to a usable input for the ADC to make a reading.

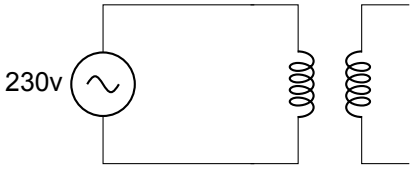

Figure 5.2: Transformer

The voltage transformer can be chosen based on the desired turn ratio for the design. If a $1:1$ turn ratio transformer were used, the two output terminals would still have a potential difference of V_{in}. It is preferred to use a higher turn ratio for down-converting the voltage to a saver range. For example, the BLOCK VB1.5/2/6 features a 230 V RMS input and two 6V RMS outputs. Another problem is introduced when using transformers, due to their inductive behavior the frequency response on higher frequencies will be different from lower frequencies. From Equation 5.1 can be taken that a higher frequency will result in a higher impedance over the transformer, making it harder for high frequencies to be transmitted to the output.

$$Z_L = j\omega L = j2\pi fL \tag{5.1}$$

After the voltage is stepped down from the mains level and isolated filtering is needed to remove high-frequency noise from the signal. This high-frequency noise will not only distort the analog signal but also alias onto the frequency bandwidth in the digital domain. To avoid the high-frequency noise effects, a low-pass filter can be used for power quality filtering. The research[29] uses an eighth-order digital low pass Butterworth digital IIR filter with a cut-off frequency of 125 Hz. It should be noted that this research uses zero-crossing detection for the power quality measurements. Zero crossing detection can determine AC characteristics, such as frequency and phase[30]. It is a requirement to determine the harmonics as well, the system is required to detect up to the 200th harmonic (Requirement S.7). The cut-off frequency is quite low, which will result in a small bandwidth, while it is desired to have a bandwidth of 10-10kHz (Requirement 3.3). Another disadvantage is that this filter is digital, while it would be beneficial to use a low pass filter before the ADC to prevent aliasing.

5.2. Applied method

Following the hardware requirement 4.2, the device should be galvanically isolated from the mains electricity network. To implement this, a voltage transformer was chosen. Requirements were that it would be able to handle a maximum of 400V AC on its primary input while outputting close to the input voltage of the ADC. Another requirement is a small form factor and low power consumption, with these requirements the Block VB1.5/6 PCB voltage transformer was chosen. In combination with a filtering and signal conditioning stage illustrated in Figure 5.3, the voltage sensor will have a suitable signal for the ADC to process.

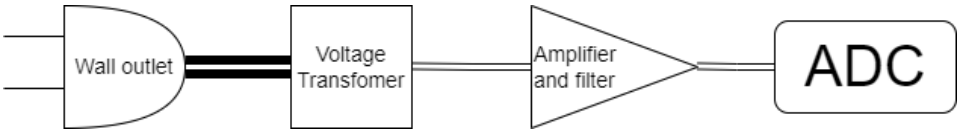

Figure 5.3: Block diagram of voltage sensor

5.2.1. Transformer

For sensing and converting the voltage the transformer BLOCK VB1.5/2/6 is used. An advantage of using this transformer is that it provides safe electrical isolation between the input and the output. This is beneficial because it prevents electrical shocks. The standard operating frequency is 50 or 60 Hz. The rated parameters of the transformer can be found in Table B.1. By using Equation 5.2 a rough

calculation can be made calculating the magnitude response resulting in $M = 0.026$.

$$M = \frac{V_{out}}{V_{in}} \tag{5.2}$$

First to get a better understanding of the transformer, an RLC test was done exposing its resistive and inductive properties. Using the technique by Abracon [31], both Magnetization and leakage inductance could be obtained with the equation $L_{total} = L_m + L_p$.
By leaving the secondary side open and connecting the RLC meter to the primary side the total inductance L_{total} can be obtained. Next, the secondary side was shorted. This lowers the output voltage to nearly zero volts, thus reducing the induced voltage in the primary windings to near zero. The displayed inductance on the RLC meter will now indicate the leakage inductance L_p. These steps are then repeated for the secondary winding measurements.[31] The obtained values can be found in Table 5.1

Table 5.1: Parameters of transformer

	Primary side	Secondary side
Total Inductance [H]	31.6	75.2m
Leakage Inductance [H]	2.63	3.55m
Magnetization inducatance [H]	29.0	71.7m
DC Resistance [Ω]	3k	5.2

Using these values a rough simplified schematic of the voltage transformer, Figure 5.4, can be made. This simplified model will be used in Subsection B.2.5 in order to determine an acceptable input resistance for the op amp filter.

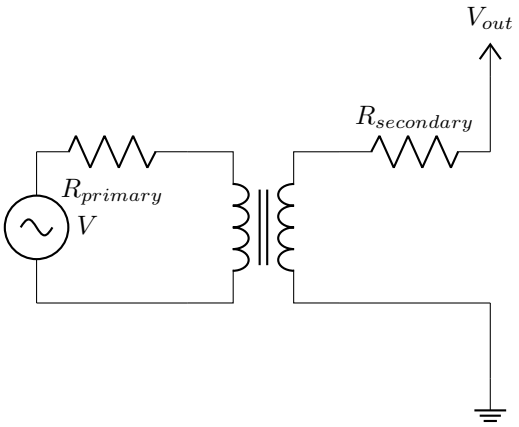

Figure 5.4: Simplified schematic of voltage tranformer

Figure 5.5 illustrates the magnitude response over the different tested frequencies. For the setup and the measurement, see section B.1

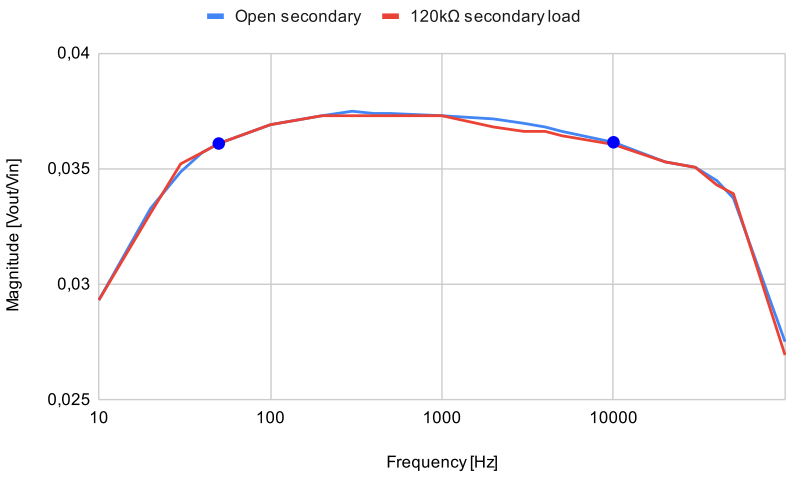

Figure 5.5: Frequency response of the BLOCK VB1.5/2/6 transformer, the two blue dots indicating 50Hz and 10kHz[32]

The frequency response shows a higher magnitude response than was calculated using the datasheet (0.036 in comparison to 0.026). This can, however, be because the transformer was not loaded during these tests. By drawing current from the secondary side the voltage of the transformer might drop to the 6V RMS specified in the datasheet.[32]
The next test was to measure the voltage transformer with a small load attached to its secondary windings. This was done because the windings will have a growing impedance as suggested in Equation 5.1. From the test results in Figure 5.5 can be concluded a high impedance ($120k\Omega$) load does not significantly influence the frequency characteristics of the voltage transformer. The graph also shows the voltage transformer is near linear in its operating frequency range between $50Hz$ and $10kHz$.

5.3. Filtering and signal conditioning

In order to measure up to a line-neutral voltage of $\pm 400V$ with the magnitude response mentioned in Subsection 5.2.1 the output voltage of the transformer will measure $2 \cdot 400V \cdot 0.036 = 28.8V$. This needs to be converted to the input voltage range of the ADC together with an offset in order to acquire a voltage range between 0.0V and 3.3V. The signal thus needs to be multiplied by a factor of $\frac{3.3V}{28.8V} = 0.1146 = H(50Hz)$. However, the Class S requirements (Requirement 3.1 mentions the device should be capable of measuring up to 120% of U_{din}. This would mean the signal conditioning circuit should attenuate by at least $\frac{0.1146}{1.2} = 0.0955 = H(50Hz)$ with an offset of $1.65V$.
Additionally, to prevent aliasing, a low pass filter is needed, with a bandwidth of $10kHz$ (Requirement 3.3).

5.3.1. First order filter

In the initial phase of the project, a first-order filter was used for its simplicity and to test if this approach would even obtain valid results, see Figure 5.6. The resistor R_1 and the capacitor C_1 will act as a high pass filter. The capacitor C_1 acts as a decoupling capacitor, which filters out low frequencies and lets the desired signal through[33]. Adding the decoupling capacitor effectively makes the filter a band pass filter. The resistors R_1 and R_2 determine the gain. The calculated component values can be found in Table 5.2, the used values in Table B.3.

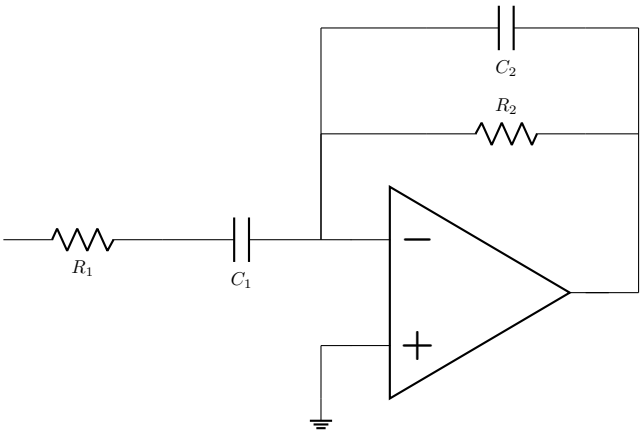

Figure 5.6: First order low pass filter

Table 5.2: Component values of LPF

Component	Value
R_1	200 kΩ-220kΩ
R_2	30 kΩ-33kΩ
C_1	200 nF
C_2	200 pF -220pF

The simplified transfer function can be found in Equation 5.3a. The DC gain K is 0.15. The cut-off frequency can be calculated with Equation 5.3b, this is done in subsection B.2.1. The intended cut-off frequency is 26.5 kHz, however, when using the real component values it ends up being 22.5 kHz. With this cut-off frequency, Requirement 3.3 is met, however a higher order filter would introduce a sharper roll-off.

$$H_{simplified}(s) = -\frac{R_2}{R_1(1 + jwR_2C_2)} \tag{5.3a}$$

$$f_c = \frac{1}{2\pi R_2 C_2} \tag{5.3b}$$

5.3.2. Second order filters

Two advantages of higher order low pass filters are a steeper slope after the cut-off frequency and a sharper phase shift. Both of which are desirable in this design, thus the first order filter is replaced by a higher order filter. Two common options exist for second-order filters: Multiple feedback and Sallen-Key. However, the Sallen-Key configuration only allows gains above 1, thus a Multiple feedback (MFB) filter is preferred since the desired gain should be around 0.0955 as calculated in Subsection 5.3. The frequency response, quality factor, and cut-off frequency calculations are displayed by equations Equations (5.4a) to (5.4c) respectively. DC gain can be calculated by inserting $\omega = 0$ in Equation 5.4a, resulting in $H(0) = \frac{-R_2}{R_1}$.

$$H(s) = \frac{\frac{-R_2}{R_1}}{s^2(R_2R_3C_1C_2) + s(R_3C_1 + R_2C_1 + \frac{R_2R_3C_1}{R_1}) + 1} \tag{5.4a}$$

$$Q_{factor} = \frac{\sqrt{R_2R_3C_1C_2}}{R_3C_1 + R_2C_1 + R_3C_1(-K)} \tag{5.4b}$$

$$FSF \times f_c = \frac{1}{2\pi\sqrt{R_2R_3C_1C_2}} \tag{5.4c}$$

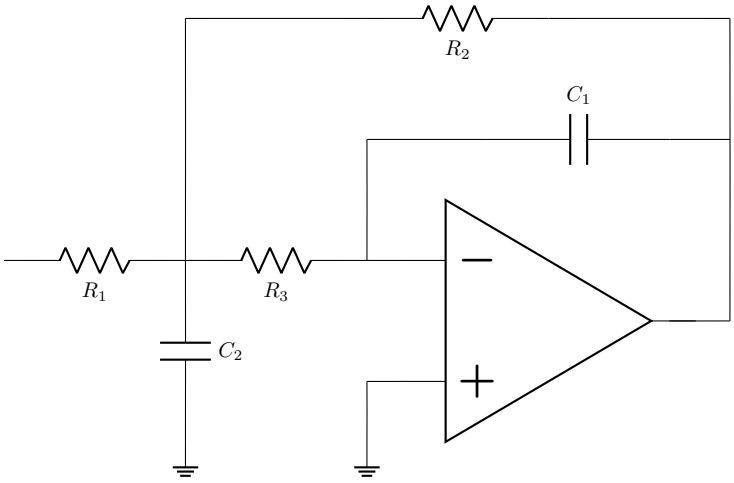

Figure 5.7: MFB active filter circuit [34]

Component selection

Since an MFB filter features two capacitors and three resistors, boundary values for these components have to be set. Capacitor values should preferably not be too big, to reduce size and cost. However, too small and the capacitance of traces and wires will start to influence the circuit. Capacitance below $100pF$ should generally be prevented when using larger THT components.[35]

Input impedance

Resistors depend highly on their placement in the circuit, however R_1 should not have too small of a resistance to keep the input impedance high. This is the preferred behaviour of a probing circuit. The frequency characteristics of a transformer is discussed in Section 5.1. Since the inductance is measure to be at $71.7mH$, the impedance at the maximum frequency of $10kHz$ will be $Z_L = |j2\pi\omega L| = |2\pi \cdot 10^4 \cdot 71.7 \cdot 10^{-3}| = 4.51k\Omega$ The input impedance of the amplifier should be at least an order of magnitude higher for it to not influence the output of the voltage transformer. Thus, a value of $50k\Omega$ or larger is preferred. To be on the safe side for this prototype, a value of $R_1 = 120k\Omega$ was chosen. Testing this resistance on the output of the secondary windings of the transformer showed no significant change in the frequency response, as discussed in Subsection 5.2.1.

DC Gain

From the value of R_1 and the chosen amplification factor, the value of R_2 can be calculated by the formula $R_2 = R_1 \cdot H(0) = 11.5k\Omega$. The final chosen value is $R_2 = 10k\Omega$. This brings down the peak-to-peak voltage further to ensure some headroom for the ADC and op amp in case components have large deviations.

Quality factor

The next design choice would be to find a suitable Q-factor. This parameter describes the peaking behaviour of a higher-order filter at the cut-off frequency. A graphical illustration of this phenomenon is shown in appendix J A Q-factor of $\frac{1}{\sqrt{2}}$ is called critically dampened, however, a higher Q-factor will result in a sharper slope for the phase response. A downside to this is that at the cut-off frequency a peaking behaviour will take place, so a compromise must be made.

The parameters of the MFB filter can be found in Table 5.3. For the lower frequencies up to nearly the cut-off frequency, the denominator in Equation 5.4a will equal to unity.

Table 5.3: MFB Parameters

Parameters	Voltage Sensing
K	-0.0833
Q_{factor}	0.998
f_c [kHz]	18.9

The ideal values that are used for the MFB filter can be found in Table 5.4, the real values are in appendix table .

Table 5.4: Component values of MFB filter

Component	Value
R_1	120 kΩ
R_2	10 kΩ
R_3	4.7 kΩ
C_1	560 pF
C_2	2.7 nF

5.3.3. SNR

ADC

The signal to noise ratio SNR is the ratio between the desired signal and the noise. A high SNR would mean that the signal amplitude is high in comparison to the noise amplitude. The signal to noise ratio of the ADC chosen in Chapter 4 is 71.5 dB. This is considered to be excellent, according to [36]. With the signal to noise ratio the effective number of bits ENOB can be calculated with Equation 5.5. For the selected ADC this results in an ENOB of 11.58bits.

$$ENOB = \frac{SNR_{real} - 1.76}{6.02} \tag{5.5}$$

Op amp

From the op amp datasheet can be read that the input voltage and current noise sources are equal to $e_n = 6nV/\sqrt{Hz}$ and $i_n = 0.9pA/\sqrt{Hz}$ respectively. For a bandwidth of $10kHz$ that would imply noise sources of $v_n = 60\mu V$ and $i_n = 9nA$ at the op amps' input. IEC 61000-3-3 states that the maximum impedance of $0,24 + j0,15\Omega$ for phase wires and $0,16 + j0,10\Omega$ for neutral wires at 50/60Hz frequencies.[37] Thus a roundtrip source to the source has the maximum impedance of $|Z_p + Z_n| = 0.47\Omega$. The parameter m is the coupling factor of the transformer, which has been measured in Subsection 5.2.1 to be $m = 0.036$. Donaldson provides an equation calculating the SNR of source connected to a voltage transformer and op amp circuit in Equation 5.6a.[38]

Since the v_n^2 term in Equation 5.6a is magnitudes larger than the $4kTR_{source}m^2$ and $(i_nR_{source})^2m^4$ terms the equation can be simplified to Equation 5.6b.

Going back to the Requirement 3.2, the maximum voltage error allowed is $0.15\%U_{NOM}$. This would mean a voltage error of $230 \cdot 0.15/100 = 0.345V$. Using this as the v_{source} and calculating the SNR with the derived formula 5.6b results in an SNR of 46.8 dB. Using Equation 5.5 to calculate the effective number of bits needed to digitize this signal, a value of $ENOB = 7.4$ calculated. Implying the voltage sensor does not yet meet the SNR of 61.96 required to have a 10 bit resolution. Measures can be taken to obtain a higher SNR, an obvious one being to reduce the noise source on the op amp input. Precision op amps feature lower than 1nV input noise source, this could be a solution to this problem. Increasing the transformer coupling factor would increase the signal level while maintaining the same noise voltage on the op amp, however high voltages are not desirable on the secondary side of the circuit.

$$SNR \propto \frac{v_{source}m}{\sqrt{v_n^2 + (4kTR_{source})m^2 + (i_nR_{soruce})^2m^4}} \tag{5.6a}$$

$$SNR \propto \frac{v_{source}m}{v_n} = \frac{v_{source}m}{60\mu V} \tag{5.6b}$$

$$m = \sqrt{\frac{R_n}{R_{source}}}, with\ R_n = \frac{v_n}{i_n} \tag{5.6c}$$

5.4. Test results

The voltage sensing was tested by both LT-spice simulation and testing the components on soldering board with high and low voltages. Reasons for chosing the LT1630 op amp in the first place was the

package size, early testing was done using bread, and matrix boards. Low noise op amps are generally contained in a SMD package.

5.4.1. Simulations

Preliminary test were done using the LTspice simulator[39]. This software gave useful insight into op amp operation and circuit simulation. Especially parameter such as quality factor and roll of are easier to quantify when using a simulation rather than simulations.

5.4.2. Second order filter

The circuit as discussed in Appendix 5.3.2 was tested with a function generator and an oscilloscope in order to obtain the frequency response. The tests were conducted using a $V_{pp} = 6,000$, offset =1,65V on the function generator. The oscilloscope was then set to measure the peak to peak voltage at the output of the MFB filter. The test results from 10Hz until 40kHz is shown in Gigure 5.8. Between 10kHz and 20 kHz a small peak appears as the filter is underdamped with a quality factor of $Q = 0.998$. After this peak a $-40dB/dec$ slope is observed cutting the higher from the signal.

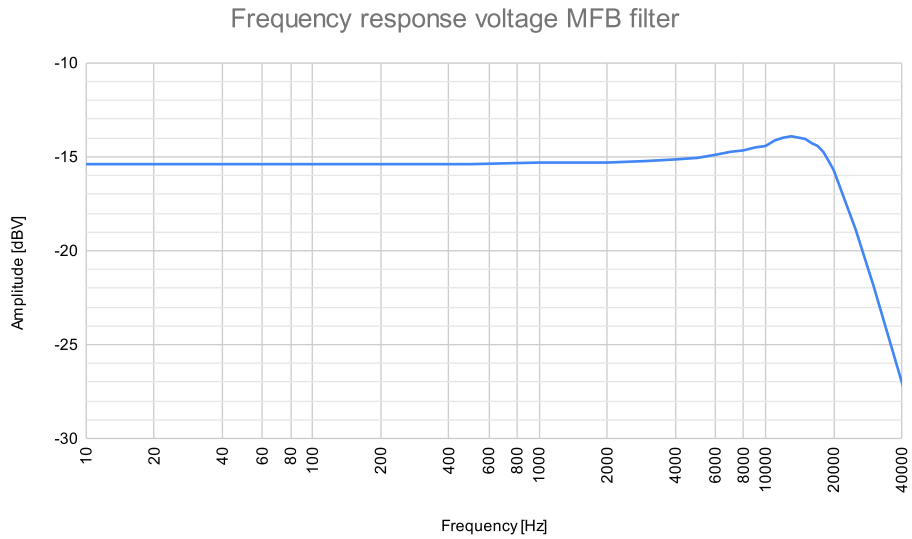

Figure 5.8: MFB filter frequency response

5.4.3. Low voltage measurements

When the individual filter tests were complete, integrated tests with the voltage transformer were performed. These test illustrate the final characteristic of the circuit before the sampling of the ADC. Before testing with high voltage, low voltage test were conducted. During these tests no major safety precautions had to be taken, that would be import for high voltage tests. The low voltage frequency response of the transformer had already been measured in Subsection 5.2.1.

Taking into account that the transformer had a different ratio from the rated ratio, the error of X1 was small. It can be seen that for the output X2 the voltage varies somewhat for the very small input voltages, but at a larger input voltage, the output voltage is better. For the input voltage of 10 Vpk-pk the final output of the op amp was as was expected, with a small error of 0.9%. Therefore it could be concluded that the voltage sensing circuit worked as was expected for low voltage tests.

Second order filter circuit

PCB voltage sensing was tested on low voltages on the MFB filter, the setup can be found in subsection B.2.4, the results and expected values can be found in Table 5.5. The block diagram of the voltage sensing module can be found in Figure 5.9.

Table 5.5: Voltage sensing output PCB (low voltage)

	Measured RMS Voltage	Expected RMS Voltage	**Error [%]**
Input Vin	7.16 V	7.07 V	1.3
Output circuit Vout,vs	22.3 mV	23.1 mV	3.5

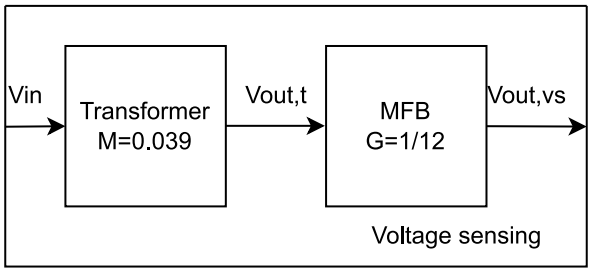

Figure 5.9: Voltage sensing block

The measured input V_{in} is a little higher than the expected RMS value, an error of 1.3%. The transformer is supposed to have a magnitude response M of 0.026, but in the transformer tests, it appeared that the magnitude response M is 0.036 at 50 Hz. The output of the transformer can be calculated with Equation 5.7a, which result in $V_{out,t} = 0.2769V$
The expected output of voltage sensing can be calculated with Equation 5.7b, which takes the gain of the MFB filter $\frac{1}{12}$ into account and results in $V_{out,vs} = 23.1mV$. The measured voltage of output circuit is 22.3 mV. The error between the measured and expected value can be calculated with Equation C.2, the error of the output circuit is 3.5%. The errors are very small and it can be concluded that voltage sensing works as expected, as long as the error are linear and thus have the possibility to calibrate.

$$V_{out,t} = V_{in,measured} \cdot M \tag{5.7a}$$
$$V_{out,vs} = V_{out,t} \cdot G \tag{5.7b}$$

5.4.4. High voltage measurements

In order to safely test the experimental device at mains voltages, a circuit breaker was used (see chapter 7).

Transformer

As a first test, the primary windings of the transformer were connected to the power outlet. The input voltage was measured by connecting a multimeter to the secondary windings. It was found that the input voltage RMS was not exactly 230 V, it varied from 229.7 V to 231.6 V during the test. The output RMS and pk-pk voltages were measured with the oscilloscope. The measured voltages were $8.84V_{RMS}$ and $25V_{Pk-Pk}$ respectively.

These results were not in accordance with the datasheet of the Block VB1.5/2/6 transformer, at an input voltage of $250V_{RMS}$ the output voltage was supposed to be 6V.[32] However during the low voltage testing already a magnitude response of 0.036, which is in accordance with the 8.84V output. However if the secondary side of the transformer were to be attached to a load, a current would be flowing allowing for the internal inductance and resistance to lower the output voltage.

More extensive high voltage test, containing harmonics, are done in Chapter 8.

6

Current sensing

The purpose of the current sensor is to measure the current flowing through the circuit to the load and express this as an analog voltage signal which is suitable for the ADC. Requirements 3.1 to 3.4 are used to guide the development throughout this chapter. This chapter first discusses the approach taken by other studies to achieve this and then is followed by an explanation of the chosen approach. Afterwards, the design process for the sensor circuit is discussed including signal conditioning and simulating. Finally, the testing results of the circuit are discussed.

6.1. Preliminary Research

Table 6.1 contains a performance comparison of different methods that can be used to measure current. This information can be used to determine the best method for measuring current for the desired application and complies with the set requirements. The initial approach was to use a current transformer to measure current. The advantages of using a current transformer are that it scales down the voltage, provides galvanic isolation and it's possible to safely monitor the output current [22]. The current transformer CoilCraft CS1750L was considered, however, there were a few issues with this transformer. For example, the frequency bandwidth was not adequate. The CS1750L is a high-pass frequency transformer, designed for use above 20 kHz, while the desired measured bandwidth is between 10 Hz and 10 kHz (Requirement 3.3). Therefore, another approach is required.

Using Table 6.1, it can already be determined that the shunt resistor and copper trace options would not meet the requirements as they lack galvanic isolation. From the remaining options and considering requirement 3.4, the current only goes above 16A for a short duration in the case that the fuse does not instantaneous blow, therefore the fiber-optic current sensor would also not be used as its range starts in kilo-amps. Additionally, it is desired for the current sensor to work even when smaller loads are used which only draw currents in the order of milli-amps, therefore the only remaining options that meet the requirements are fluxgate, core-less open-loop, or GMR, AMR, and Hall effect sensors with temperature compensation. Of these options, fluxgate would be the most desirable as it meets these requirements and has a much higher accuracy compared to the other options.

Table 6.1: Comparison of different methods to measure current taken from "Current Sensing Techniques: A Review" [40]

	Bandwidth	DC Capable	Accuracy	Thermal drift $[\mathrm{ppm/K}]$	Isolated	Range	Power Loss
Shunt Resistor • Coaxial • SMD	MHz kHz-MHz	Yes	$0.1\% - 2\%$	$25 - 300$	No	kA $\mathrm{mA - A}$	$\mathrm{W - kW}$ $\mathrm{mW - W}$
Copper Trace [1]	kHz	Yes	$0.5\% - 5\%$	$50 - 200$	No	$\mathrm{A - kA}$	mW
Current Transformer	kHz-MHz	No	$0.1\% - 1\%$	< 100	Yes	$\mathrm{A - kA}$	mW
Rogowski Coil	kHz-MHz	No	$0.2\% - 5\%$	$50 - 300$	Yes	$\mathrm{A - MA}$	mW
Hall Effect [1] (open-loop / closed-loop)	kHz	Yes	$0.5\% - 5\%$	$50 - 1000$	Yes	$\mathrm{A - kA}$	mW
Fluxgate	kHz	Yes	$0.001\% - 0.5\%$	< 50	Yes	$\mathrm{mA - kA}$	$\mathrm{mW - W}$
AMR Effect [1] (closed-loop, core-less)	kHz	Yes	$0.5\% - 2\%$	$100 - 200$	Yes	A	mW
Core-less open-loop (GMR, AMR, Hall Effect) [1]	kHz	Yes	$1\% - 10\%$	$200 - 1000$	Yes	$\mathrm{mA - kA}$	mW
Fiber-Optic Current Sensor [1]	kHz-MHz	Yes	$0.1\% - 1\%$	< 100	Yes	$\mathrm{kA - MA}$	W

[1] Using temperature compensation electronics

6.2. Selected Current Transducer

The current transducer selected is the CASR 15-NP developed by LEM. All subsequent information regarding this component is obtained from the datasheet provided by LEM [41]. This current transducer is designed using a closed-loop fluxgate design and is galvanically isolated (Requirement 4.2). The transducer has a maximum input primary current of $\pm 51A$, which is an RMS current of $36.06A$, thus this transducer meets Requirement 3.4. The $\pm 1dB$ bandwidth of this transducer is 200 kHz which also meets Requirement 3.3. The theoretical sensitivity is $41.67mV/A$ and the transducer has an accuracy between 0.8% and 1.2% of the primary nominal current which is relevant for Requirements 3.1 and 3.2. Additional benefits of this transducer are that it is powered using a $5V$ power supply, which is convenient since the Raspberry Pi and op amps operate on the same voltage. The transducer also features a $2.5V$ reference pin output to be used in the subsequent signal conditioning sections.

Preliminary tests were done with the current transducer using direct current before continuing with circuit design. This can be found in Appendix C.

6.3. Circuit Design

6.3.1. Signal conditioning

The analog input range of the ADC (as has been discussed in Section 4.3) is $0V$ to $3.3V$ and has a resolution of 12 bits. Using rough calculations, the smallest increment of power consumption can be calculated. For this calculation assume the highest RMS current is 16A (Requirement 3.4), although the breaker would not immediately blow, and the RMS voltage is $230V$. The lowest current increment is determined by dividing the current by the number of increments, thus $16/(2^{12})$ which equals $3.90625mA$. Multiplying this value by $230V$ results in the lowest average power consumption increment of 0.898 watt. This could be improved through multiple methods. Two potential methods could be the use of programmable gain amplifiers (PGA) or logarithmic amplifiers. However both offer their own challenges. PGA's require close collaboration between software and hardware, assuming there exists an ADC with a built-in PGA that also satisfies the other requirements. Logarithmic amplifiers feature a logarithmic current range, compressing the higher current, while keeping high accuracy on the low currents. However, log amplifiers are often temperature dependant and difficult to calibrate.[42] Instead, it was decided to implement two separate circuits with different gain factors, one for low current sensing (up to 2A rms) and the other for high current sensing (above and beyond 16A rms). Doing the same calculation as previously but using 2A rms instead of 16A results in the lowest average power consumption increment being 0.1123 watt. Therefore, this method would allow for higher accuracy for devices with a lower average power consumption. Requirement 3.2 also tells that the accuracy for current lower than 10% of the nominal current needs to be within $\pm 0.5\% I_{nom}$. For a nominal current of $16A_{RMS}$ this implies an accuracy of $\pm 80mA$.

To determine the gain factor for the low current sensor, the rms value is converted to peak to peak by multiplying the RMS value by $2\sqrt{2}$ which results in a peak-to-peak current of $5.656A$. Using the

sensitivity of the current transducer mentioned in Section 6.2, the output of the current transducer is determined to be $235.72mV$. This output is then filtered (which will be discussed in Section 6.3.2) and then used as an input for an op amp. The gain is calculated to use the entire output range of the op amp which is $5V$. Dividing the maximum output of the op amp by the peak-to-peak output of the transducer results in an ideal gain factor of 21.21 for the low current sensor.

The same approach can be taken to determine the gain factor of the high current sensor. The max RMS value is taken as twice the circuit breaker rating, so $32A$ RMS. This converts to $90.5A$ for peak-to-peak current. Once again using the current transducer sensitivity gives a maximum peak-to-peak output of $3771mV$. The gain calculated is then 1.325.

The op amp used is the same as that for the voltage sensor. This op amp has a maximum output of $5V$ and will be reduced to $3.3V$ using a resistor divider before the input of the ADC. The current transducer conveniently has a 2.5V reference pin which is used at the input of the op amp. Voltage division occurs after the op amp such that the maximum output of the op amp does not exceed the analog input range of the ADC as opposed to voltage division occurring before the op amp, where the output of the op amp could damage the ADC.

6.3.2. Filtering

For consistency, the same MFB filter topology as used in Section 5.3 is used for the High and low current measurements. However different gain factors, as discussed in Subsection 6.3.1, and input impedances could be selected because the CASR 15-NP current transducer features a built-in op amp. According to the datasheet, a minimum load resistance on the output should be $1k\Omega$.[41] The circuit schematic of the current sensing module can be found in Figure 6.1. Here the two different sub-circuits can be seen for the low and high current sensors. Note that the filter topology for both of these sub-circuits is the same as that of the MFB filter for the voltage sensor (Subsection 5.3.2). The calculated filter parameters and component values for these filters can be found in Table 6.2 and B.3 respectively. The ideal gain factor for low current sensor is 21.21, for high current sensor it is 1.325. The used values vary a little from the ideal signal conditioning values, by 0.7% for the low current sensor and 35.8% for the high current sensor.

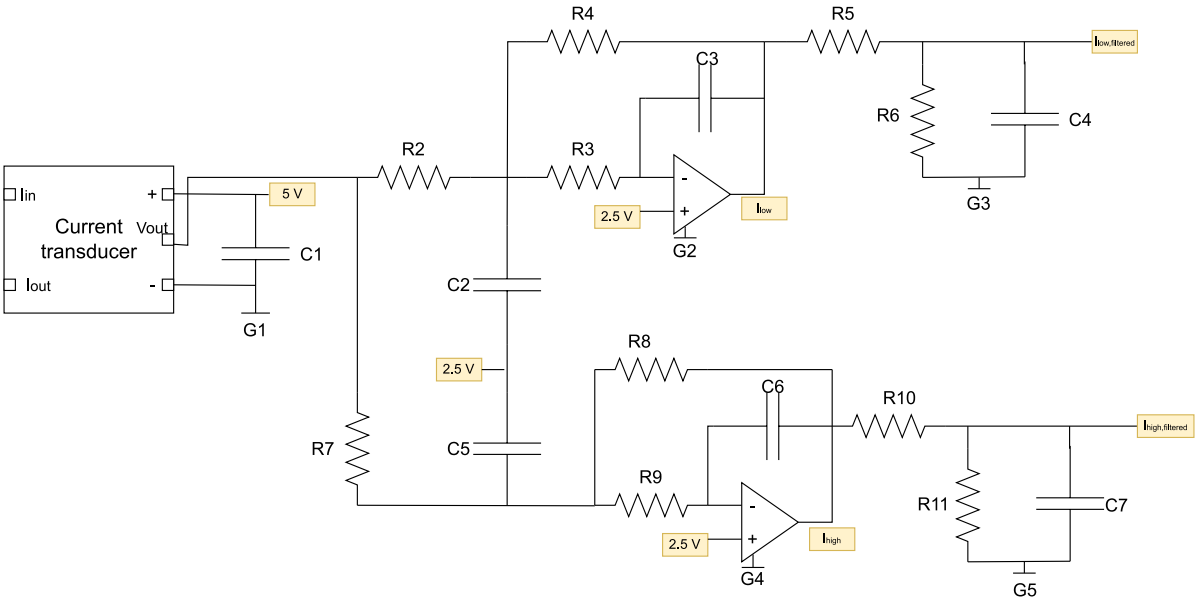

Figure 6.1: Current Sensing Circuit Schematic

Table 6.2: Parameters current sensing

Parameters	Low Current Sensing	High Current Sensing
K	-21.36	-1.8
Q_{factor}	0.902	0.936
f_c	21.1 kHz	18.9 kHz

6.3.3. Spice simulations

Before building the circuit, simulations were made to validate the circuit design. Figure 6.2 illustrates the frequency response of both the low and high current measurements and their cut-off frequency. A slight ramping-up phenomenon is visible just before the $-40dB/dec$ dropoff, due to the increased quality factor. This is a compromise that needs to be made between gain and phase response. The phase experiences a sharper shift because of the increased quality factor of 0.902 for the lower current sensor and 0.936 for the high current sensor.

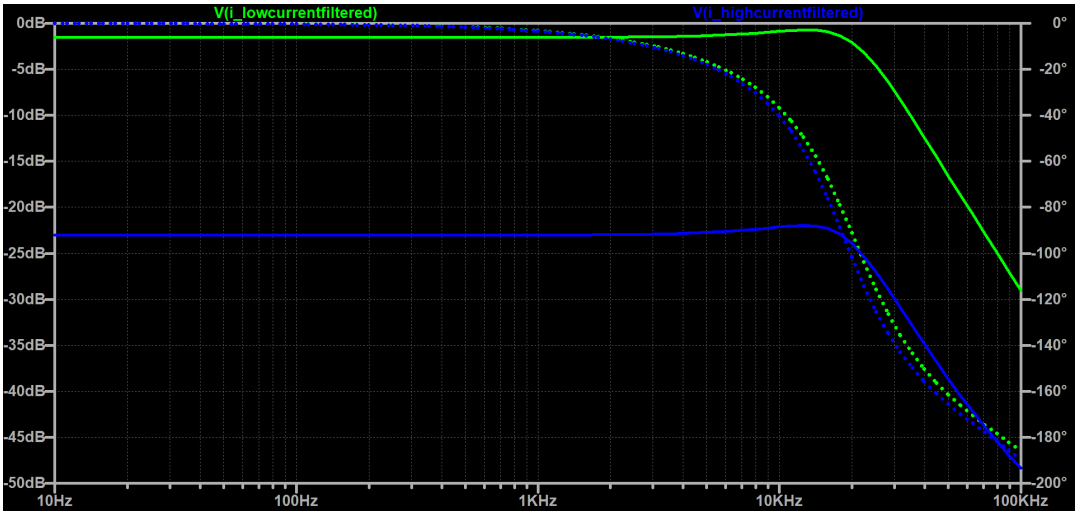

Figure 6.2: Frequency and phase response of the low (green) and high (blue) current MFB filters

Live waveform data shows another aspect of the circuit. Figure 6.3a shows the low current sensor operating at a $1A_{RMS}$ sine wave signal. While the low current almost saturates the input range of the ADC, the high current MFB circuit only supplies a very small signal. Figure 6.3b shows an increased current draw of $10A_{RMS}$. With this current the low current MFB filter will go into saturation mode, while the high current filter outputs an uncompromised sign wave to the ADC. The importance of these two signals has been explained in Chapter 4.

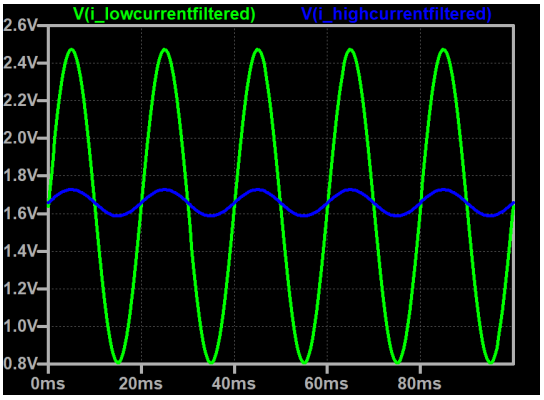

(a) $1A_{RMS}$ current simulation

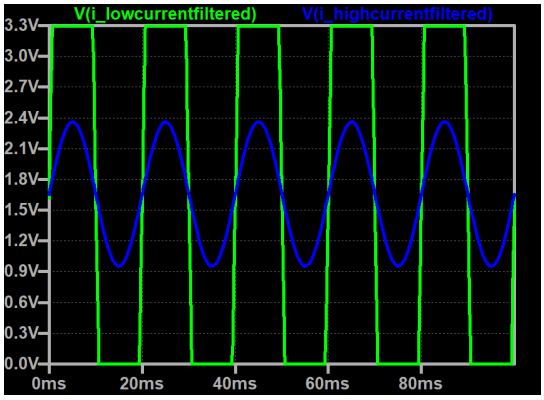

(b) $10A_{RMS}$ current simulation

Figure 6.3: Simulation of low (green) and high (blue) current MFB filter using LTspice[39]

6.4. Current Sensor Testing

6.4.1. Low-Current Sensing

The low-current sensor was tested first. The measurement setup can be seen in Figure D.1 in Appendix D. An AC signal was produced using a function generator, however, the function generator did not have enough power to generate a sufficient current to test the current sensor. Therefore, a power amplifier circuit intended for audio systems was used to amplify the test signal. It is important to note that the amplifier circuit did have a high pass filter with a cutoff below 200 Hz, thus a signal of 300Hz was used during testing rather than 50 Hz. A $\pm 18V$ power supply was used to power the amplifier circuit. This setup was able to deliver an RMS current of 2 amps to a 5Ω load which was sufficient for testing the low-current sensor. The results of this testing can be seen in Figure 6.4, where the RMS current is plotted against the voltage output of the op amp. As can be seen, this relationship is relatively linear except for an RMS current above 2A where the output saturates at 3.3V. This was done intentionally as the max analog input range of the ADC is 3.3V, thus the entire range of the ADC input is used over the 2A RMS current range.

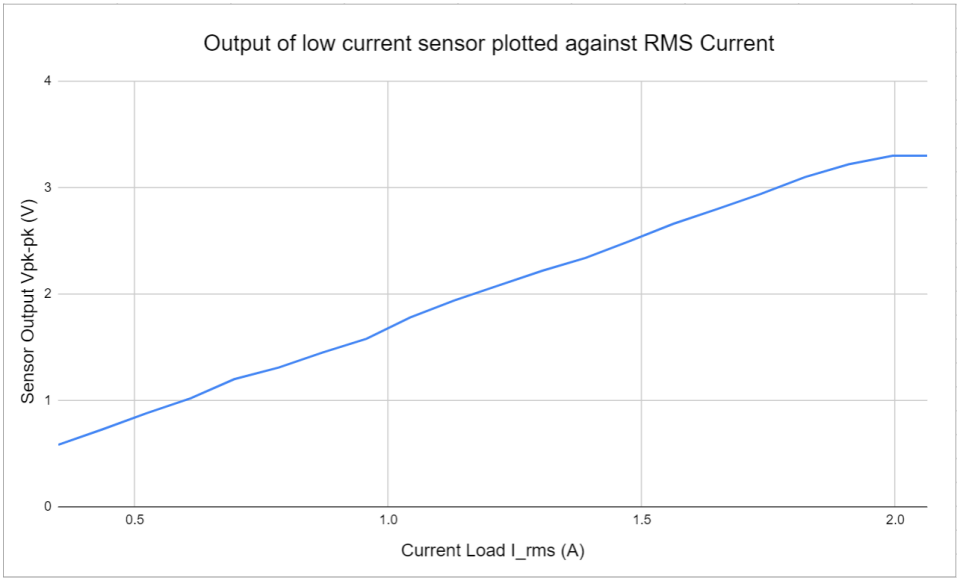

Figure 6.4: RMS current plotted against low-current sensor output

6.4.2. Low current tests PCB

The PCB current sensing was tested for low currents using the same setup which can be found in Figure D.3. In Figure 6.5 the block diagram of the low current sensing module can be found.

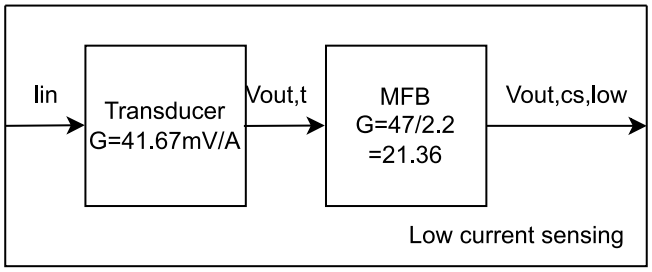

Figure 6.5: Low current sensing block

In Table 6.3 the results of low current tests can be found. This is a summary of the results that were obtained, for the complete overview of the results, see Table D.1. The measured I_{RMS} is given, Ch2 is the output RMS voltage of the current sensor. The measured and expected output of the current sensor are compared. It can be seen that there is a error of approximately 5% for the output of the

current sensor. A very accurate low current sensing output. It should be noted that the input of I_{RMS} of 2.008A there occurred clipping. While the current error is significant at around 5%, it seems to have a consistent error allowing for calibration of the sensor.

Table 6.3: PCB test for low current sensor

Measured input I_{RMS} [A]	Measured output [V]	Expected output [V]	Error [%]
0.334	0.197	0.196	5.15
0.5	0.295	0.294	5.31
0.666	0.392	0.391	5.63
0.831	0.488	0.488	6.02
0.996	0.594	0.585	4.67
1.16	0.692	0.681	4.8
1.33	0.793	0.781	4.55
1.499	0.893	0.881	4.45
1.667	0.993	0.979	4.38
1.843	1.1	1.083	3.7
2.008	1.18	1.18	5.31

6.4.3. High Current Sensing

The measurement setup for the high-current sensor can be seen in Figure D.2 in Appendix D. The measurement setup required a high-power AC source which was procured and overlooked by a supervisor. This source was able to provide more than the 16 amp RMS current required to test the sensor. Figure 6.6 contains the results from testing. Testing occurred across an RMS current range from $0.76A$ to $18.8A$. The result was a relatively linear relationship with the nonlinear issues most likely being a result of the source used as harmonics were present in the source at certain current levels. The voltage output at $18.8A$ was $2.54V$. This is not close to the maximum analog input of the ADC, however, this was done intentionally as the fuses do not immediately blow at 16A. Therefore, some input range was reserved for overcurrent events above 16A such that these events could still be measured. Further current test were done once the device was completed, these results can be found in Chapter 8.

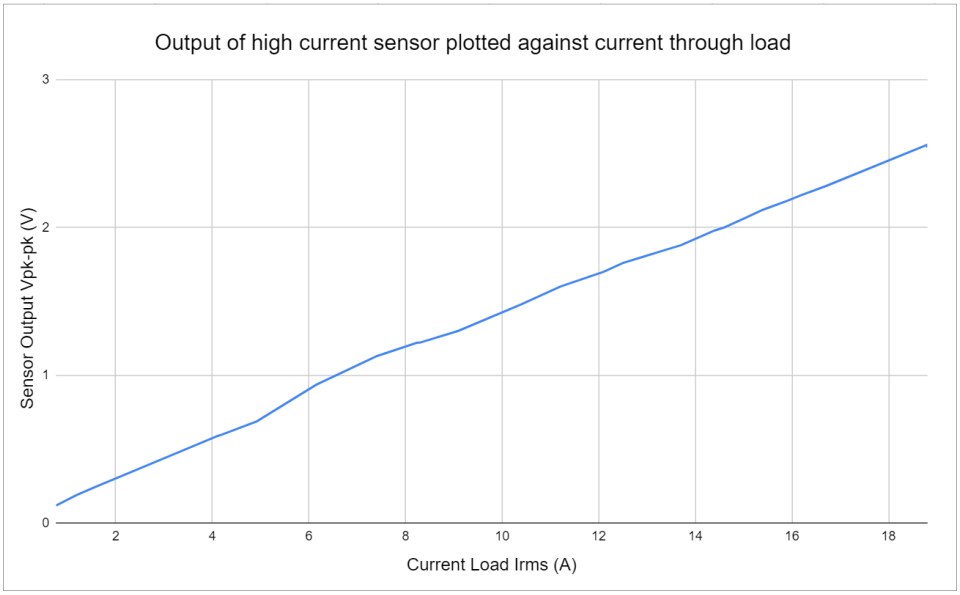

Figure 6.6: RMS current plotted against high-current sensor output

7

Safety and Protection

7.1. Safety

In order to perform measurements safely while testing with mains voltage, our supervisor Remko Koornneef, provided a circuit breaker. The schematic of the circuit breaker can be found in Figure H.1. It was placed between the voltage source (the mains) and the voltage sensing circuit, as indicated in Figure 7.1. This device could be used to turn on the power on a Type F socket while providing protection using 10-ampere fuses.

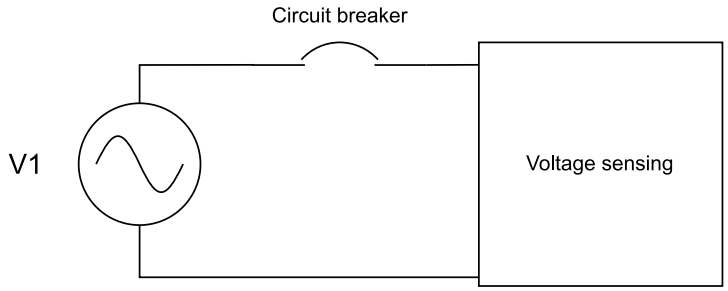

Figure 7.1: Setup for testing high voltages

A 3D-printed enclosure for the product (which includes the PCB and Raspberry Pi) has been made for safety purposes (Requirement 4.1). The main purpose of the enclosure is to prevent any exposed terminals from potentially causing harm to the user, hence the use of non-conducting screws to hold the lid and internal components in place. The enclosure also serves as a physical barrier, shielding the internal components from potential damage. See Figure G.1 for the printed enclosure of the product.

Another important safety consideration taken into account is that the circuit must be galvanically isolated (PoR 4.2). This was done by selecting components for the voltage and current sensor which provided galvanic isolation for the circuit as discussed towards the beginning of Chapters 5 and 6 respectively.

7.2. Protection of the circuit

Requirement 4.3 states that the product should be protected. Overcurrent, overvoltage, and thermal protection will be discussed.

7.2.1. Overcurrent protection

Overcurrent occors when the current through a device exceeds the rated current, which may damage components.
Ways to prevent the circuit from overcurrent events is to use circuit breakers or fuses. Circuit breakers trip (interrupt the current flow) when a fault such as an overcurrent is detected. Standardized Type F

power sockets support a maximum RMS current of 16A, 3560W.[43] The device is specifically made for household applications, ensuring that it restricts the flow of current through a breaker to a maximum of 16A. As mentioned before, fuses can be used for overcurrent protection as well. A fuse contains a fuse element which is a wire that is designed to burn when a certain current passes through it leaving an open circuit that stops current flowing. The fuse is installed before the device, to protect the other components from the excessive current [44] as can be seen in Figure 7.2. The rate at which the fuse burns can be chosen: it can burn slow, fast, or in between. Slow-burning fuses do not burn immediately when an overcurrent is occurring. Some inrush or transient current can be detected before the slow-burning fuse burns up when the duration is longer. Fast burning fuses burn up immediately when the overcurrent occurs [45]. The chosen fuse is a 16A slow acting fuse and is able to detect overcurrent events. The cables that were used, and other components in the current pathway are all able to withstand sustained current flows of 16A. Since the fuse is the weakest link in this chain, it will be the first point of failure.

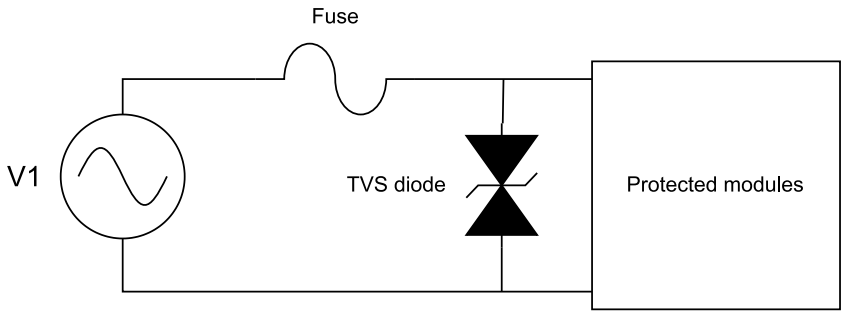

Figure 7.2: Protection

7.2.2. Thermal protection

In the circuit heat dissipation occurs when power is not efficiently transmitted, and power is lost to heat. This might lead to high temperatures which can damage the components. The transformer is an inherently short-circuit proof transformer. This means that ”In the event of overload or short-circuit and in the absence of any protective device, the transformer does not exceed the specified limits and can operate normally after removal of the overload or the short circuit” [46]. The current transducer has a maximum RMS current withstand capacity of 36.06 A. Given that the current is expected to be at most 16 A, the current transducer is well within its safe operational range, ensuring protection from excessive heat generated by the current.

Inside the enclosure, the temperature could increase reducing performance and damaging components. For this reason, vents for airflow were included in the enclosure design and a heat sink has been installed on the Raspberry Pi to improve thermal exchange and prevent overheating.

7.2.3. Overvoltage protection

To protect the device from high voltages, some over-voltage protection should be added. Specifically, the device should be protected from transients. Texas Instruments shows the different types of surge protection devices that could be used.[47] The table of the properties is shown in Table 7.1 Based on these properties, the decision was made that the Transient Voltage Suppression (TVS) diode offers distinct advantages compared to the other types of surge protection devices. For example, it is less affected by light and it offers a long lifetime and reliable voltage regulation. It is not economically wise to use a TVS diode for high currents. However, a fuse (which prevents the current flow to 16A) is placed in front of the TVS diode, as is indicated in Figure 7.2. It is quite important to place the fuse in front of the TVS diode. This is because a shorted TVS device can become dangerous when conducting current through the return path [47]. TVS diodes work according to the Avalanche effect. In the event of a high-energy transient overvoltage pulse, its working impedance is reduced to a very low conduction value. This allows the maximum current to pass through and clamps the voltage to a predetermined level. As a result, components within the circuit are protected from damage [47]. However, the TVS diode does need to dissipate these high energy bursts in the form of heat, sustained transient or overvoltages are thus not recommended in combination with a TVS diode. TVS diodes can be unidirectional or bidirectional [47]. In this scenario, choosing a bidirectional TVS diode was essential

due to the placement of the component on an AC line.

A filter was proposed to be a good solution to prevent high-frequency transients from passing through[47]. It is a cheap solution and it will result in a better, low-noise signal. The low pass filter that is chosen is an MFB filter, see chapter 5 and chapter 6 for the parameters.

Table 7.1: Transient Suppression Component Types [47]

Type of Surge Protection Device	Description	Advantages	Disadvantages
Gas Discharge Tube	Gas between two plates that is ionized to carry current during a large voltage spike	Highest power dissipation density and very low capacitance	Long turn on time, light sensitive behavior, large footprint, and poor voltage regulation
Metal Oxide Varistor (MOV)	Mass of metal grains that creates a diode like breakdown	High power dissipation density	Poor voltage regulation, finite life expectancy, catastrophic breakdown mechanism, and poor thermal dissipation
Thyristor	Diode like behavior but with a snapback profile to limit power dissipation	High power dissipation density due to snapback behavior	Chance of latch-up breakdown
Transient Voltage Suppression Diode	Avalanche breakdown diode behavior to shunt current to ground	Decent power dissipation density, long lifetime, and good voltage regulation	Not economical at high $(> 250\ \mathrm{A})$ current dissipation
Filter	Passive components to filter out high frequency transients	Cheapest solution	Very low power dissipation density

7.3. PCB

In order to meet Requirements 3.4 and 4.3 the device should handle $16A_{RMS}$ and $400V_{Peak}$. Using a prototyping board like a breadboard or matrix board no guarantee can be made that these requirements are met. Another problem with these basic boards is the circuit will be very difficult to troubleshoot due to its growing complexity. Thus, in order to mitigate these problems, the decision was made to design a PCB.

7.3.1. PCB trace width

In order to let a $16A_{RMS}$ current flow through the circuit,the IPC-2221 standard provides useful equations in order to calculate the trace width. Online tools were used in order to calculate the minimum trace width for a $35\mu m$ thickness, $50°C$ temperature rise carying $16A$ of current. The resulting trace thickness was $13.5mm$. Since this trace size together with a trace clearance discussed in Subsection 7.3.2 will result in a big spacing between connector pins, the decision was made to route the current carrying trace both on the top and bottom side of the PCB. Both top and bottom layer having a with of $7mm$.

7.3.2. PCB trace clearance

Safety standard UL 60950-1 states the functional isolation of a 250VAC system requires a $1.5mm$ trace spacing. The IPC-2221B safety standard uses a more generous spacing, however since the device does not require electric shock protection a less strict standard may be used. Different rules apply when bringing a product to the consumer market, together with product testing.

8

Integrated system test results

Having tested all the individual components and filters, the next step is to assemble the modules and test the integrated system. Both the accurate operation of the voltage and current parts need to be validated.

A grid simulator was used to test the voltage sensor. This simulator can produce a 50Hz sign wave at a selectable amplitude, as well as generate harmonics within this signal. In this section no load was yet connected, this will be done in Section 8.3.
During the first test, a 50Hz sign wave signal without harmonics was used on the input of the power quality analyzer. Results of this first test are shown in Figure 8.1a. Channel 1 (yellow) is the output of the voltage sensor and channel 2 (blue) is the output of the high current sensor. These signals are the input for the ADC. Using a multimeter, the RMS voltage on the input was measured at $233.6V_{RMS}$. Interestingly, a signal was generated by the current sensor while no load was attached. However, since the internal cables connecting the grid input to the PCB route over a major part of the circuit (Figure G.2, interference can be induced in these components. Solutions to this problem are discussed in Chapter 9.

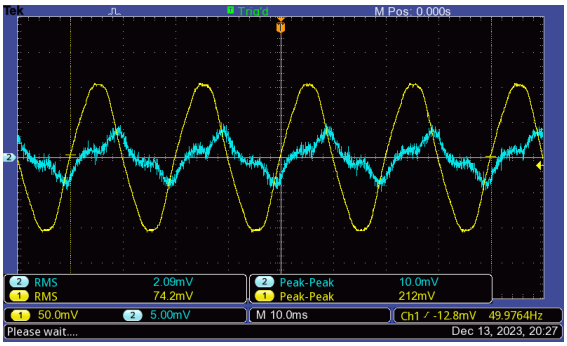

(a) Test 13

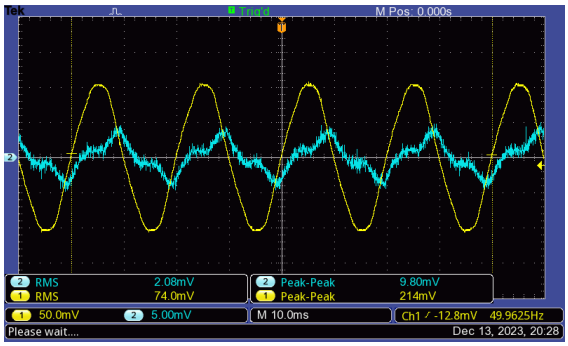

(b) Test 14

Figure 8.1: Integrated device test with no load attached. Inteference is noticable on the current sensor (blue), while the voltage sensor (yellow) seems to operate nominally

8.1. Voltage Harmonic Tests

For measuring the voltage harmonic sensing capabilities the grid simulator was configured to have both the primary harmonic H1 (50Hz), and one or multiple additional frequencies. Table 8.1 displays the voltage levels at which the Harmonics occur.

Table 8.1: Harmonics tested

Harmonic	Test 1	Test 2	Test 3	Test 4
H1	220 V	220 V	220 V	220 V
H5	0 V	1 V	10 V	10 V
H7	0 V	0 V	0 V	5 V
H19	0 V	0 V	0 V	2 V
H29	0 V	0 V	0 V	1 V

The setup can be found in Figure I.8 Data from this test setup was recorded using an oscilloscope and frequency spectrum graphs were made using the Matlab code in Appendix F. The graphs of the measured harmonics can be found in Figure I.9, the graphs of the frequency spectrum are shown in Figure 8.2

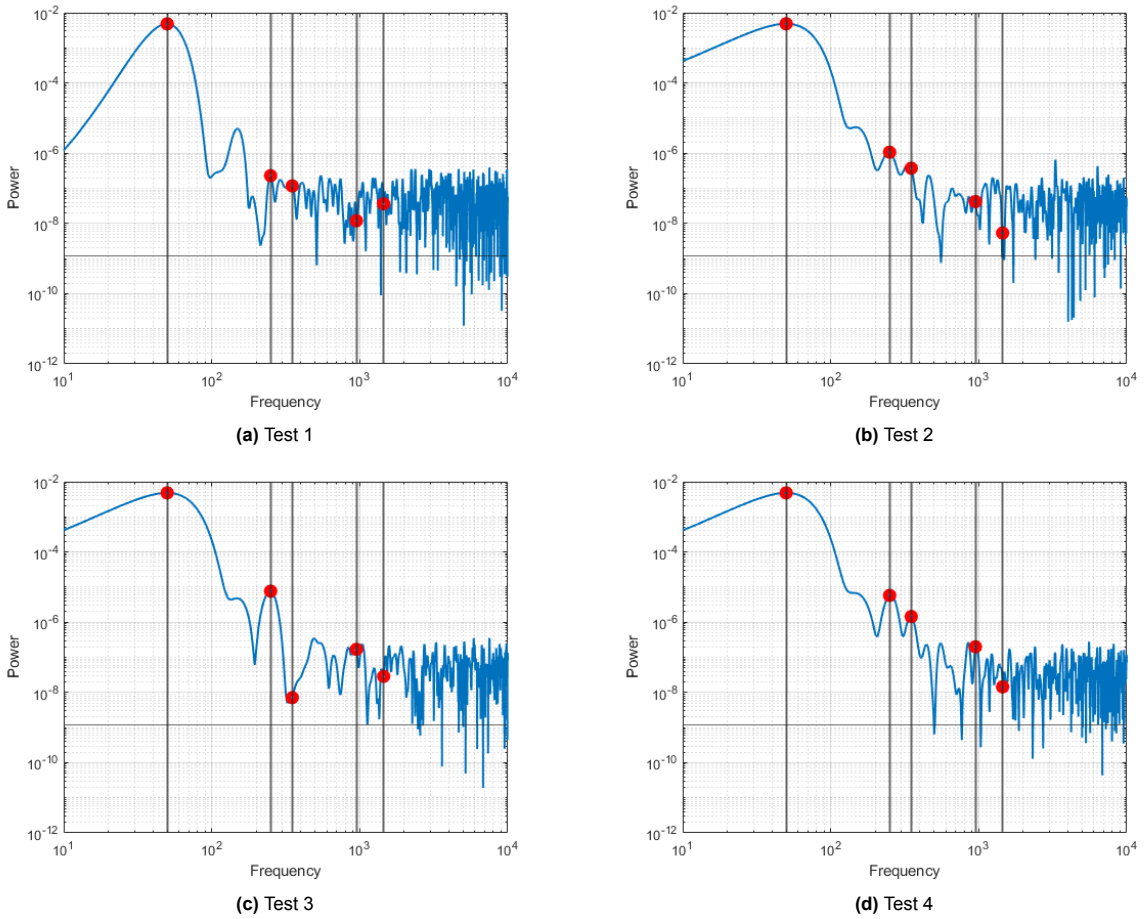

(a) Test 1

(b) Test 2

(c) Test 3

(d) Test 4

Figure 8.2: Harmonic testing, the black horizontal line illustrates the minimum accuracy the voltage sensor should acquire. The vertical lines illustrate the harmonic frequencies from Table 8.1 at 50, 250, 350, 950, 1450Hz.

As a baseline test a signal of $220V_{RMS}$ was used on the input of the voltage sensor, no harmonics were introduced yet. The results from this test are shown in Figure 8.2a. The majority of the power is in the 50Hz frequency range, however a smaller peak is seen at 150Hz and 250Hz. These harmonics can be introduced either by the grid simulator, the voltage sensor or the cables in between. Extensive testing would need to be done to find the source of this harmonic.
The second test only has one harmonic at a 250Hz and $1V_{RMS}$, the results are displayed in figure 8.2b. During this test the side lobes of the 50Hz signal are significantly wider than during the first test. This makes it seem like the 150Hz frequency has been reduced, however it is now partly contained in the

side lobes. The 250Hz frequency has had a significant boost in power.
The third test was a repetition of the second, however this time the fifth harmonic has a $10V_{RMS}$ signal. In Figure 8.2c a clear distinction can be made between the 250HZ and 350 Hz frequencies.
The final test contained a total of four harmonics on top of the original 50Hz signal, now both 250 and 350 Hz peaks are visible, however the higher frequency peak at 950Hz an 1450Hz are still hard to see. Keep in mind the amount of data supplied for these samples was only 2500 data points over a timespan of $50ms$.

8.2. Resistive Load Test

Measurements using the same grid generator as mentioned previously are done. However, now a resistive load is connected through the power quality analyzer. The load in question is a $2500W$ electric hotplate. The setup can be found in Figure I.4. This hotplate was tested on three settings: the low setting which draws 4.4A. The medium setting draws a larger current of 6.4A and the high setting draws an even larger current of 10.A. Note that the high current sensor is measured as the lowest current tested already exceeds the input range of the low current sensor. The graph of the output of the channels on the oscilloscope of the low current setting is shown in Figure 8.3.

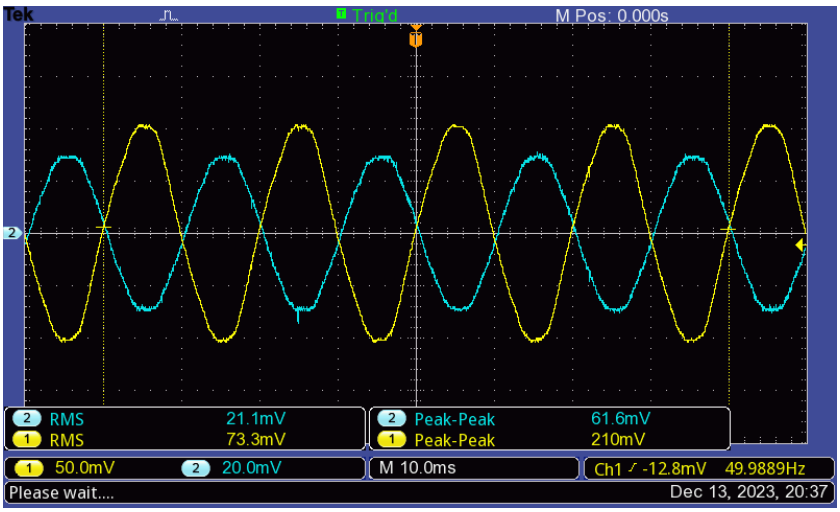

Figure 8.3: Test on low setting of hot plate, CH1 (Yellow) Output of voltage sensor, CH2 (Blue) Output of high current sensor

The graphs of the medium and high power setting can be found in Appendix I.2. To get a clear overview of the results, some of the results are repeated in Table 8.2. It can be seen that the error between both channels is within 0.5%. Since the current flowing through a resistive load is proportional to the voltage applied to the load, a 4% increase in grid voltage would contribute to a 4% increase in current flow. For channel 1, the voltage sensor the maximum error is 4%, for channel 2, the current sensor, the maximum error is 3,6%. Since the voltage is raised, the current is thus also expected to have a higher reading.

Table 8.2: Results of measurements of various loads

Picture	Description	Real Ch1 [mV]	Expected Ch1 [mV]	Error Ch1 [%]	Real Ch2 [mV]	Expected Ch2 [mV]	Error Ch2 [%]
15	Hot plate (low)	733	756,9	-3,2	211	217,8	-3,1
16	Hot plate (medium)	730	756,6	-3,5	307	316,8	-3,1
17	Hot plate (high)	722	752,4	-4	513	495,0	3,6

8.3. Various Load Tests with entire system

After assembling the device, sample measurements of resistive loads, such as a hot plate or industrial lamps, and switch mode power supplies, such as laptop chargers and battery chargers, were recorded using the entire system (all modules including Raspberry Pi) to represent a use-case application of the device. Additionally, these tests were done while powering the device from the mains voltage. Only one voltage recording is included in Figure 8.4 as the load attached does not have a significant impact on the mains voltage reading.

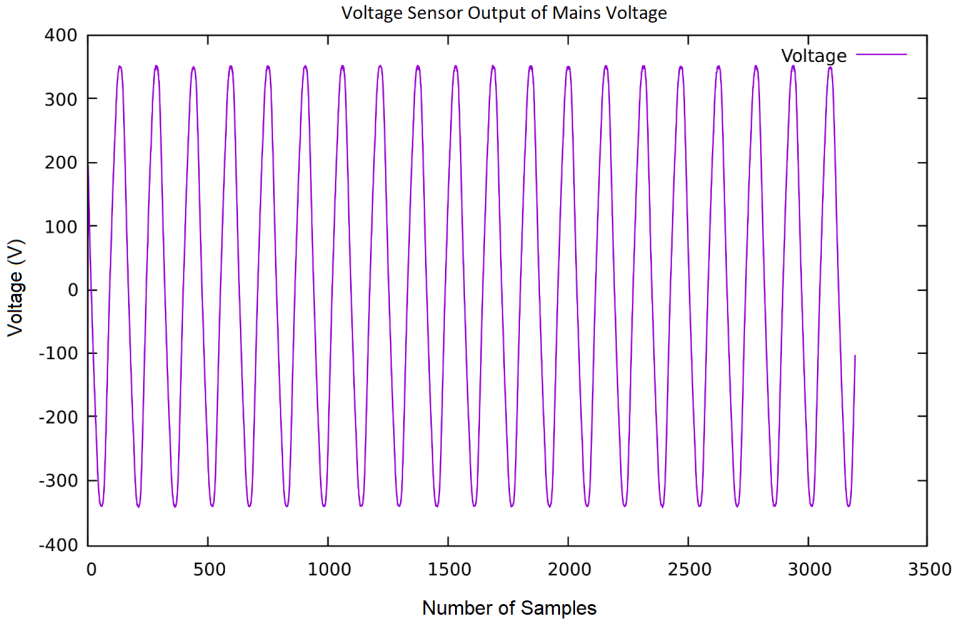

Figure 8.4: Recording of the voltage sensor output with the device plugged into the mains voltage

To begin with, current sensor measurements using an industrial work lamp can be found in Figure 8.5. The current measured by the low current sensor resembles a relatively clean 50 Hz sinusoidal signal as expected from a resistive load. On the other hand, the high current sensor is more sensitive to noise at lower currents, and thus the peaks of the sinusoidal signal experience some interference. This can be expected due to the higher gain of the high current sensor.

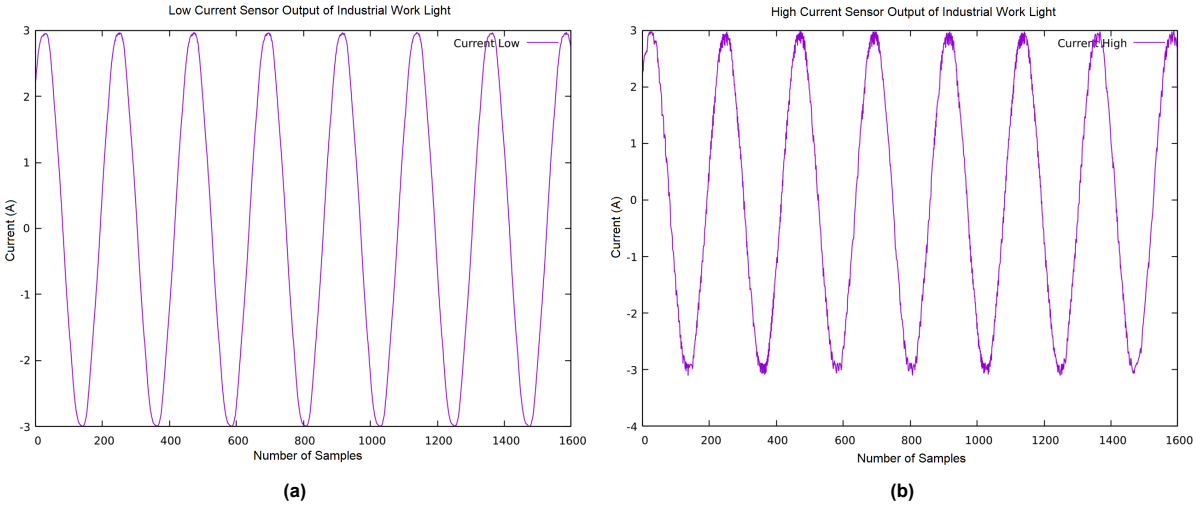

Figure 8.5: Recording of current sensor outputs with an industrial work light as the load

Afterward, a laptop was plugged into the device and charged. The current measurements for this load

can be found in Figure 8.6. As expected, the waveform is significantly distorted from the original sinusoidal signal due to the switch mode power supply. The high current waveform once again experiences interference due to the relatively low current being drawn.

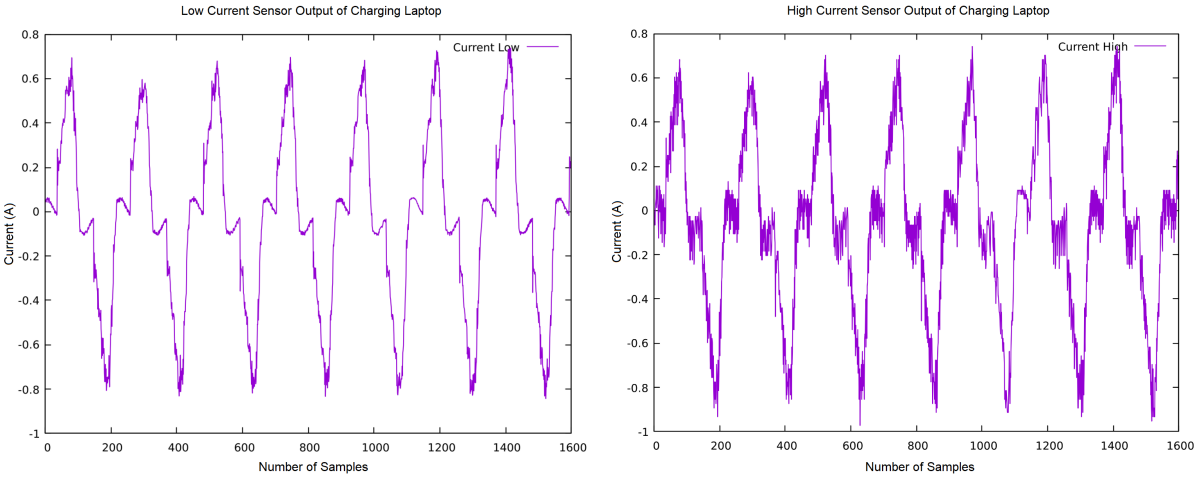

(a) (b)

Figure 8.6: Recording of current sensor outputs with a charging laptop as the load

The measurements shown in Figure 8.7 demonstrate what occurs when a current larger than the designed range of the low current sensor is being measured. This is done by using a power strip to attach an industrial work light and two charging laptops simultaneously. It can be seen that the current exceeds the range of the low current sensor as the peaks of the signal experience clipping. In comparison, the high current sensor can measure this increased current without issue. It can also be seen that the high-current sensor still experiences some interference at the peaks of the signal.

Additionally, an important observation that is easy to overlook. The slope of the low current sensor signal before the clipping occurs is no longer as smooth as before the switch mode power supplies were added to the load as shown previously in Figure 8.5a. This observation could also be made from the high current sensor measurement, although it is difficult to determine how the peaks are affected by this due to the interference present.

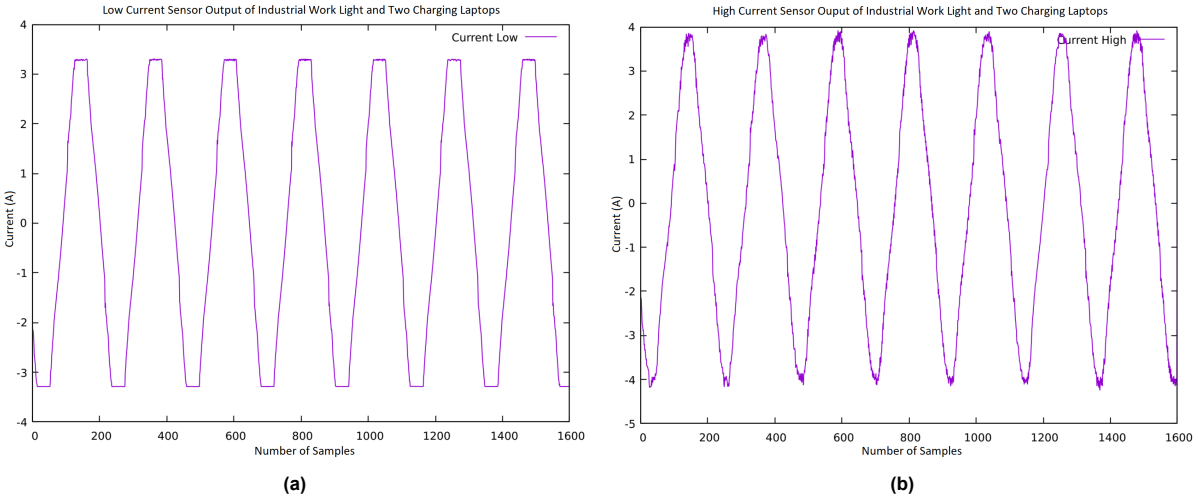

(a) (b)

Figure 8.7: Recording of current sensor outputs with an industrial work lamp and two charging laptops as the load

Finally, an additional work light is added to further increase the current drawn by the load. These measurements are shown in Figure 8.8. Once again, the increased current exceeds the range of the

low current sensor as seen by the more extreme clipping. Additionally, the interference experienced at the peaks of the high current sensor signal is still present. The magnitude of the interference present in the high current sensor appears to be consistent across the different load configurations further reinforcing the speculation that this is caused by noise.

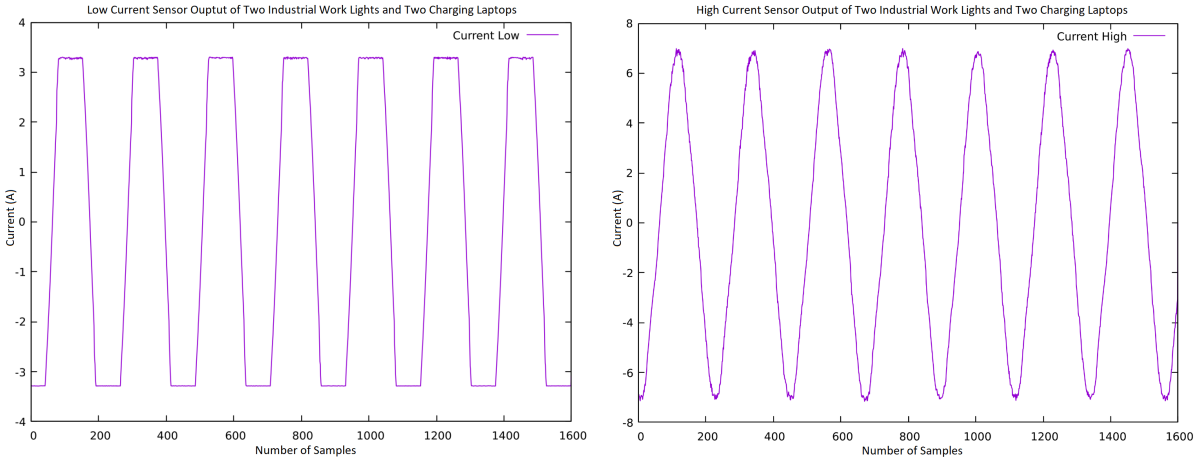

(a) **(b)**

Figure 8.8: Recording of current sensor outputs with two industrial work lamp and two charging laptops as the load

9 Discussion

In this section, the requirements will be evaluated as to whether or not they have been achieved followed by a discussion of the future improvements which could be carried out to further improve the prototype.

9.1. Evaluation

The hardware-specific requirements will be evaluated first as these were derived from the system requirements, followed by an evaluation of the system requirements themselves. Note that the system requirements will be evaluated independently of the performance of the software subgroup.

9.1.1. Evaluation of Hardware Requirements

Requirements 1.1 and 1.2 pertain to the device layout. Photos of the final product are shown in Appendix G. As can be seen by Figure G.1, only one plug is required to power the system and take measurements. Additionally, a socket is present for a load to be connected. Therefore both of the design layout requirements are met.

As for the device functionality requirements, the results in Section 8.3 demonstrate that the prototype is capable of voltage and current waveform detection, as well as carrying these functions out independently of each other. These measurements were taken while the device was plugged into a single-phase system operating at 230V RMS at 50 Hz (mains electricity). Thus it can be concluded that the device functionality Requirements 2.1, 2.2, and 2.3 have been met.

The device has been designed with consideration of the class S requirements (Requirements 3.1 and 3.2). For instance, the current accuracy stated by the Class S Accuracy Standards (Table 2.2) was the reasoning for the current sensor being separated into a low and high current sensor. However, insufficient testing was done to determine whether these requirements were met.

The voltage transformer, current transducer, and filters were selected and designed such that the operating bandwidth was from 10 Hz to 10 kHz. Therefore Requirement 3.3 has been met for the individual modules but has not been tested for the entire system. Additionally, testing of the high current sensor was done in Section 6.4.3 to demonstrate that the device can operate and perform measurements in a system with a breaker of 16A (Requirement 3.4).

Requirements 4.1, 4.2, and 4.3 specify what needs to be done to keep the device and its user safe. This is thoroughly discussed in Chapter 7 and from this, it can be concluded that these have been achieved although testing would be required to determine the effectiveness of the circuit protection implemented. Lastly, the ADC was carefully selected such that Requirements 5.1, 5.2, 5.3, and 5.4 were met.

As for the trade of requirements, a PCB was designed for the circuit (ToR.1). The system was then assembled onto the PCB before system testing occurred. The remaining trade requirements are suggested as future improvements in Section 9.2

9.1.2. Evaluation of System Requirements

As determined from the evaluation of the hardware requirements, the device is capable of recording voltage and current waveforms independently and thus should be able to meet system Requirements S.1 and S.2. Additionally, as the device can operate on a 16A breaker, it meets system Requirement S.3.

Unfortunately, as mentioned previously, it has not been determined that the device meets the specifications of a Class S power quality analyzer (Requirement S.7) due to insufficient testing.

As for the design process, the system was designed in separate modules and a Raspberry Pi 4 Model B was implemented (Requirements S.4 and S.5. The ability of the device to store a month of data recordings (Requirement S.6) is dependent on the software subgroup, however, a 128GB micro SD card was chosen such that the software team had a large amount of memory storage available without significantly increasing the total assembly costs.

Lastly, as can be found in Appendix K, the total cost of components required to produce this prototype is €224.38. This was also calculated using the costs of buying the minimum number of each component necessary. Buying the components in bulk would further reduce the costs of production per unit, therefore it can be determined that Requirement S.8 has been met.

9.2. Future Improvements

It would be naive to assume there were no faults made throughout this project. These include oversights, lack of sufficient testing, or work that could still be done. Therefore, many recommendations can be made to rectify these mistakes and further improve this project.

9.2.1. Voltage Sensor

Using a PCB voltage transformer to down-convert and isolate the primary to the secondary side of the voltage sensor may not be the most accurate implementation of a voltage sensor. Due to the nonlinear nature of the magnetic core in a transformer, the magnetic hysteresis can negatively influence the voltage transformation.[48] This phenomenon may take place when a voltage transformer is exposed to overvoltages, DC offset, or frequencies below the fundamental frequency.[49] The research: Power quality in DC distribution networks [50] uses the voltage transducer LV25-P, which is a closed loop hall effect sensor that is used for voltage measurements. While the term transducer is not specific in the way this voltage sensor works, the datasheets indicate that it has a similar operation to the CASR 15-NP current transducer. Both transducers operate with a hall effect sensor measuring the current through a winding, however, the voltage sensor will have to operate at a lower current since it is limited in power dissipation [41, 51]. The benefit of this approach is that there is no core to transmit the magnetic flux, thus no core saturation can occur. Hall effect type voltage transducers also offer capability of DC measurements, this will be discussed in Subsection 9.2.6.

9.2.2. PCB Adjustments

During the assembly of the PCB, some oversights were made and could be improved for future versions of the PCB. The mistakes that were encountered have already been fixed on the PCB design file and were not significant enough to prevent a functional prototype from being made. Some of these mistakes included a through-hole not being placed under the ADCs to connect them to the ground plate for heat dissipation, as well as not incorporating a resistor on the trace connected to the physical programmable address of the ADCs which was an issue as both ADCs were attempting to communicate to the same address (this was manually fixed for the prototype).

9.2.3. Prototype Validation

Arguably the most important step to be taken would be for more testing to be done to determine the validity of the prototype. This has been done to an extent with the individual voltage and current sensors using the testing setups described in Sections 5.4 and 6.4. However, although some measurements have been made using mains voltage, reference signals have not been thoroughly recorded to be compared to the device to determine its accuracy. Additionally, testing should be done with power quality disturbances present to determine the performance of the prototype in use-case applications,

as well as to determine whether class S requirements are met. However, a testing setup able to induce these power quality disturbances in a repeatable and accurate means at mains voltage level and power must be procured, which was only able to be done for harmonics up to this point as was discussed in Section 8.1.

9.2.4. Transient Detection

Currently, the prototype is unable to detect transients. A preliminary design for a transient detection circuit was being made, however, it was determined that it would be more beneficial to ensure other components would be designed first as transient detection is a trade-off requirement. This design could be refined in the future and incorporated into the system at a later stage.

9.2.5. Power Disruption

If a power interruption were to occur, valuable data leading up to the interruption would be lost. One solution to this could be implementing a battery between the $5V$ power supply and Raspberry Pi. This would allow the Raspberry Pi to continue recording data in the case of such an event. However, the use of a battery could also bring into question the sustainability of the device, as well as marginally increase the costs of production. Such an addition would also be more relevant if the device were to be used in environments where power interruptions are more common which was not a concern during the development of the prototype. Therefore, this is being considered as a potential future implementation.

9.2.6. DC Operation Capabilities

In order to expand capabilities DC operation could be an expansion. The setup currently used does not support DC operation, since the voltage transformer only allows for AC. The 5V power supply is able to operate on a $100 - 430VDC$ input.[52] The CASR 15-NP is capable of measuring both AC and DC signals.
A solution for the voltage sensor should thus be able to operate on both AC and DC in the specified voltage range. Suitable sensor options include the Lem voltage transducer LV 25-P and DVC 1000-P, however both come at a price significantly higher than a PCB voltage transformer. The LV 25-P features a somewhat customizable voltage input range by changing a resistor value, the DVC 1000-P does not offer this feature. However the latter is capable of measuring up until $\pm 1500V$ peak, this is well outside the range of the PoR and will thus influence the accuracy of the ADC.

9.2.7. Further Miscellaneous Testing

There were some additional concerns raised during development that could be tested further to determine the impact they have on the prototype. One such concern was noticed during testing with PCB. A soldering iron nearby was powered on and the wire powering the soldering iron was under the PCB while preliminary testing of the current sensor was in progress. As a result, the current sensor measurements had slight deviations which were fixed by turning the soldering iron off. This raises the question, if this deviation was caused by the current flowing through a wire under the PCB, would the load lines that carry a current up to $16A$ near the PCB also influence the current sensor's measurements? And would improved cable insulation be a sufficient solution to remedy this?

Additional concerns were raised related to the power supply of the circuit. Currently, all components are powered by the same source as the measurements are being made from. This leads to the question, does this cause issues with the accuracy of the measurements caused by interference and if so, how could this be overcome? Yet another concern raised is that the op amps and ADCs are powered through the GPIO pins of the Raspberry Pi. It has been observed that the Raspberry Pi draws more power when there is a higher computational load. Can this deviation in drawn power be seen on the voltages of the GPIO pins of the Raspberry Pi, and if so, how does this deviation of supply voltages of the op amps and ADCs impact the performance of these components and the accuracy of the system?

10

Conclusion

The objective of this thesis was to design the hardware for a low-cost, class S power quality analyzer intended for single-phase systems capable of detecting; harmonics, voltage sags and swells, over and under voltages, as well as measuring power factor and consumption. Requirements were set in place in order to guide the development of the device. The general approach taken during the design process began with preliminary research and component selection, followed by circuit design, assembly, and testing.

The design consisted of three modules: analog to digital conversion, voltage sensing, and current sensing. In the voltage sensing module, a transformer was employed to decouple the AC mains, providing isolation and scaling down the voltage. The MFB filter played a crucial role in further scaling down the voltage to a level suitable for input to the ADC. As for the current sensing module, a current transducer was used which provides current measurement and galvanic isolation. The module was split into a low and high current sensor for up to 2A RMS and 32A RMS respectively to improve the overall accuracy, hence two MFB filters were implemented in this module.

A functional prototype was assembled, including the development of a dedicated PCB, and use-case measurements were recorded. The prototype was able to be safely tested on single-phase systems operating at 230V RMS at 50 Hz as a result of meeting the set safety requirements. Furthermore, the total cost of the assembly for the prototype was kept below €250.00 with a total of €224.38.

Unfortunately, it cannot be determined whether or not the class S specifications have been achieved due to insufficient testing, despite design decisions being diligently made in regard to these specifications. However, this shortcoming can also be seen in a positive light. Although the class S specifications may not have been realized, the foundation for a low-cost power quality analyzer has been set which can readily be built upon.

References

[1] Transmission, Distribution Committee, et al. *IEEE Std 1100-1999 IEEE recommended practice for powering and grounding electronic equipment*. 1999.

[2] Carlo Masetti. “Revision of European Standard EN 50160 on power quality: Reasons and solutions”. In: *Proceedings of 14th International Conference on Harmonics and Quality of Power - ICHQP 2010*. 2010, pp. 1–7. DOI: 10.1109/ICHQP.2010.5625472.

[3] Kabiru A. Hassan. Daniel O. Johnson. “Issues of Power Quality in Electrical Systems”. In: vol. 5. 4. 2016, pp. 148–154. DOI: 10.11648/j.ijepe.20160504.12.

[4] J. M. A. Myrzik S. Bhattacharyya and W. L. Kling. “Consequences of poor power quality - an overview”. In: Brighton, UK, 2007, pp. 651–656. DOI: 10.1109/UPEC.2007.4469025.

[5] *Laborelec and KEMA TD Consulting Power quality op het Aansluitpunt - fase 1: inventarisatie en probleembeschrijving*. Tech. rep. Doc. No.: 40530061-TDC 05–54719 A. (available in Dutch). Feb. 2006.

[6] John A. McNeill Alexander Eigeles Emanuel. “ELECTRIC POWER QUALITY”. In: vol. 22. Worcester, Massachusetts, 1997, pp. 263–303. DOI: 10.1146/annurev.energy.22.1.263.

[7] Sarah Rönnberg and Math Bollen. “Power quality issues in the electric power system of the future”. In: vol. 29. Dec. 2016, pp. 49–61. DOI: 10.1016/j.tej.2016.11.006.

[8] M.N. Tandjaoui et al. “Role of power electronics in grid integration of renewable energy systems”. In: 16 (Jan. 2016), pp. 369–374.

[9] Michael S Witherden, Ramesh Rayudu, and Rémy Rigo-Mariani. “The influence of nonlinear loads on the power quality of the New Zealand low voltage electrical power distribution network”. In: *2010 20th Australasian Universities Power Engineering Conference*. 2010, pp. 1–6.

[10] *Power Quality Equipment Market Size, Share, Competitive Landscape and Trend Analysis Report by Equipment (UPS, Harmonic Filters, Surge Protection Devices, Voltage Regulators, Static VAR compensators, Others), by Phase (Single Phase, Three Phase), by End User (Residential, Commercial, Industrial): Global Opportunity Analysis and Industry Forecast, 2021-2031*. Tech. rep. A15551. Aug. 2022.

[11] Eduardo Viciana et al. “OpenZmeter: An Efficient Low-Cost Energy Smart Meter and Power Quality Analyzer”. In: *Sustainability* 10.11 (2018). ISSN: 2071-1050. DOI: 10.3390/su10114038.

[12] Ewerton L. de Sousa et al. “Development a Low-Cost Wireless Smart Meter with Power Quality Measurement for Smart Grid Applications”. In: *Sensors* 23.16 (2023). ISSN: 1424-8220. DOI: 10.3390/s23167210.

[13] Mayurkumar Rajkumar Balwani et al. “Development of a Smart Meter for Power Quality-Based Tariff Implementation in a Smart Grid”. In: *Energies* 14.19 (2021). ISSN: 1996-1073. DOI: 10.3390/en14196171.

[14] Dusan Medvedr et al. “Project design of the electric power quality analyzer using an open-source platform”. In: Nov. 2018, pp. 000169–000172. DOI: 10.1109/CANDO-EPE.2018.8601160.

[15] Anthony J Christe, Sergey Negrashov, and Philip M Johnson. “Design, implementation, and evaluation of open power quality”. In: *Energies* 13.15 (2020), p. 4032.

[16] *Electrical accessories – Circuit-breakers for overcurrent protection for household and similar installations – Part 1: Circuit-breakers for a.c. operation*. Tech. rep. 60898-1. IEC, Mar. 2020.

[17] Amir Broshi. “Monitoring power quality beyond EN 50160 and IEC 61000-4-30”. In: *2007 9th International Conference on Electrical Power Quality and Utilisation*. 2007, pp. 1–6. DOI: 10.1109/EPQU.2007.4424114.

[18] *Electromagnetic compatibility (EMC) – Part 4-30: Testing and measurement techniques - Power quality measurement methods*. Tech. rep. 61000-4-30. IEC, Mar. 2021.

[19] *Electromagnetic compatibility (EMC) - Part 4-7: Testing and measurement techniques - General guide on harmonics and interharmonics measurements and instrumentation, for power supply systems and equipment connected thereto*. Tech. rep. 61000-4-7. IEC, Aug. 2002.

[20] *ADS7142-Q1 Automotive, 2-Channel, 12-Bit, 140-kSPS, I2C-Compatible ADC WithProgrammable Threshold and Host Wake-Up Features*. SBAS891B. Texas Instruments. Sept. 2022.

[21] *SAR ADC Input Types*. 0615B. Linear Technology.

[22] *Making AC Mains Voltage and Current Measurements*. https://wiki.analog.com/university/courses/tutorials/alm-awg-ac-mains-tests. Accessed: Oct 10, 2023.

[23] *Common Mode for Signal Line, Through-Hole Type, SBT-01W Series*. LF0065 SBT-01W. Version 9. LEM. Aug. 2023.

[24] *Understanding Voltage Sensors*. https://robocraze.com/blogs/post/voltage-sensor. Accessed: Oct 23, 2023.

[25] *What is Circuit Loading?* URL: `https://saving.em.keysight.com/en/knowledge/glossary/oscilloscopes/what-is-circuit-loading`.

[26] Jake Williams. “Study of Current Optocoupler Techniques and Applications for isolation of Sensing and Control Signals in DC-DC Converters”. MA thesis. Fayetteville, Ar: University of Arkansas, Dec. 2012.

[27] T.K. Hareendran. *ZMPT101B AC Voltage Sensor Module Primer*. Feb. 2022. URL: `https://www.electroschematics.com/voltage-sensor/`.

[28] Qingxian Zeming. *ZMPT101B Current-type Voltage Transformer*. URL: `https://5nrorwxhmqqijik.leadongcdn.com/ZMPT101B+specification-aidijBqoKomRilSqqokpjkp.pdf`.

[29] Nuno M Rodrigues, Fernando M Janeiro, and Pedro M Ramos. “Low pass digital filter delay compensation for accurate zero cross detection in power quality”. In: *IMEKO TC 4* (2017), pp. 407–410.

[30] *Zero Crossing Detector*. Mar. 2022. URL: `https://www.renesas.com/us/en/document/apn/1210-zero-crossing-detector`.

[31] A Alamin. “Exploring Transformer Basics Understanding Transformers: Part 1”. In: (Jan. 2021). URL: `https://abracon.com/uploads/resources/Abracon-Exploring-Transformer-Basics-Understanding-Transformers-Part-1.pdf`.

[32] Block. *VB 1,5/2/6: Safety isolating transforme*. URL: `https://www.block.eu/en_EN/productversion/vb-1526/`.

[33] *Coupling and Decoupling*. URL: `https://eepower.com/capacitor-guide/applications/coupling-and-decoupling/`.

[34] R. Mancini. *Op Amps For Everyone*. Texas Instruments Incorporated, Aug. 2002. URL: `https://web.mit.edu/6.101/www/reference/op_amps_everyone.pdf`.

[35] S.J. Sangwine. *Electronic components & technology, 2nd edition*. 2nd ed. Cheltenham, England: Nelson Thornes, June 1994.

[36] *Understand SINAD, ENOB, SNR, THD, THD + N, and SFDR so You Don’t Get Lost in the Noise Floor*. MT-003. Analog Devices. URL: `https://www.analog.com/media/en/training-seminars/tutorials/MT-003.pdf`.

[37] *Electromagnetic compatibility (EMC) - Part 3-3: Limits - Limitation of voltage changes, voltage fluctuations and flicker in public low-voltage supply systems, for equipment with rated current ≤ 16 A per phase and not subject to conditional connection*. Tech. rep. 61000-3-3. IEC, Mar. 2021.

[38] N. de N. Donaldson. “12 - Tripolar interfaces for neural recording”. In: *Implantable Sensor Systems for Medical Applications*. Ed. by Andreas Inmann and Diana Hodgins. Woodhead Publishing Series in Biomaterials. Woodhead Publishing, 2013, pp. 359–400. ISBN: 978-1-84569-987-1. DOI: `https://doi.org/10.1533/9780857096289.3.359`. URL: `https://www.sciencedirect.com/science/article/pii/B9781845699871500120`.

[39] Analog Devices. *LTspice Information Center*. 2000. URL: https://www.analog.com/en/design-center/design-tools-and-calculators/ltspice-simulator.html.

[40] Silvio Ziegler et al. “Current Sensing Techniques: A Review”. In: *IEEE Sensors Journal* 9.4 (2009), pp. 354–376. DOI: 10.1109/JSEN.2009.2013914.

[41] *Current transducer CASR series*. N°97.E6.15.000.7. Version 9. LEM. May 2017.

[42] Analog Devices. *Log Amp Basics*. 2009. URL: https://www.analog.com/media/en/training-seminars/tutorials/MT-077.pdf.

[43] IEC. *World plugs*. URL: https://www.iec.ch/world-plugs.

[44] Tony R. Kuphaldt. *Physics Of Conductors And Insulators*. All about circuits. URL: https://www.allaboutcircuits.com/textbook/direct-current/chpt-12/fuses/.

[45] components101. *Choosing between Slow Blow and Fast Blow Fuse for Power Circuit Protection*. May 2020. URL: https://components101.com/articles/choosing-between-slow-blow-and-fast-blow-fuse-for-power-protection.

[46] Feb. 2021. URL: https://www.bimectrasformatori.com/en/company/standards-and-certifications/.

[47] *How to select a Surge Diode*. SLVAE37. Texas Instruments. Jan. 2019.

[48] J. Dong. *EE2C11: Power Factor and Harmonics*. URL: https://jianning.info/course/ee2e11/reader/power_factor_harmonics.html.

[49] Sarath Perera and Sean Elphick. “Chapter 7 - Implications of equipment behaviour on power quality”. In: *Applied Power Quality*. Ed. by Sarath Perera and Sean Elphick. Elsevier, 2023, pp. 185–258. ISBN: 978-0-323-85467-2. DOI: https://doi.org/10.1016/B978-0-323-85467-2.00002-0. URL: https://www.sciencedirect.com/science/article/pii/B9780323854672000020.

[50] Julio Barros, Matilde de Apráiz, and Ramón I Diego. “Power quality in DC distribution networks”. In: *Energies* 12.5 (2019), p. 848. URL: https://www.mdpi.com/1996-1073/12/5/848.

[51] Dec. 2022. URL: https://www.lem.com/sites/default/files/products_datasheets/lv_25-p_v21.pdf.

[52] RS PRO. *Datasheet: PCB mount Switch Mode Power Supplies*. URL: https://docs.rs-online.com/0432/A700000008294855.pdf.

[53] Electronics Tutorials. *Sallen and Key Filter*. URL: https://www.electronics-tutorials.ws/filter/sallen-key-filter.html.

A

ADC

A.1. ADC datasheet

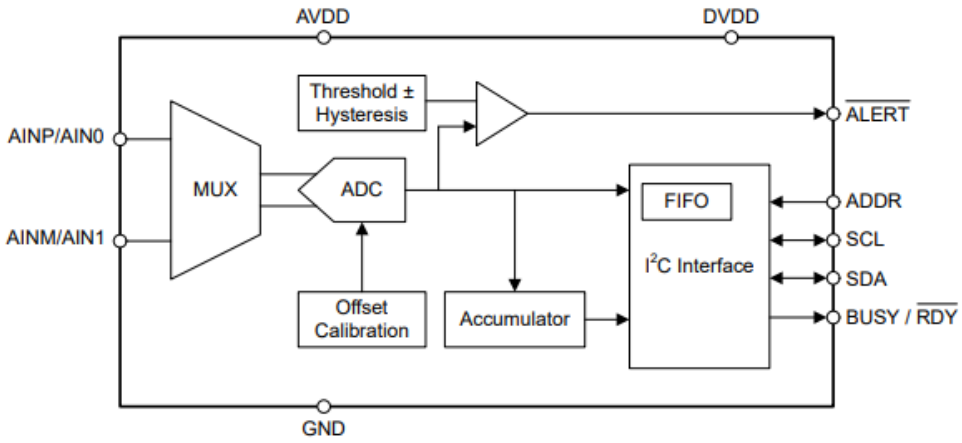

Figure A.1: Block diagram of AD7142-Q1 [20]

B

Voltage Sensing Testing

B.1. Transformer

The rated parameters of the transformer can be found in Table B.1

Table B.1: Rated parameters transformer

Frequency [Hz]	Input voltage [V]	Output voltage [V]	Magnitude response
50	230	6	0,02608695652

The frequency response was measured by varying the frequency from 10 Hz to 100 kHz of the input signal of the function generator. The input voltage was set to 20 V peak to peak. The output voltage of the transformer was measured using the first channel of an oscilloscope, while the second channel was used for referencing the input signal to the transformer. This was necessary due to the inductance of the transformer changing the impedance over the different measured frequencies. The magnitude response M is calculated with Equation 5.2. The results can be found in Table B.2

Table B.2: Transformer measurements

Frequency [Hz]	Input voltage pk-pk [V]	Open secondary voltage pk-pk [mV]	M	Input voltage pk-pk [V]	120 kohm load voltage pk-pk [mV]	M
10	17,2	504	0,0293	17,2	504	0,0293
20	19,6	652	0,0333	19,6	648	0,0331
30	20,2	704	0,0349	20	704	0,0352
40	20,4	728	0,0357	20,4	728	0,0357
50	20,4	736	0,0361	20,4	736	0,0361
100	20,6	760	0,0369	20,6	760	0,0369
200	20,6	768	0,0373	20,6	768	0,0373
300	20,6	772	0,0375	20,6	768	0,0373
400	20,6	770	0,0374	20,6	768	0,0373
500	20,6	770	0,0374	20,6	768	0,0373
1000	20,6	768	0,0373	20,6	768	0,0373
2000	21	780	0,0371	21,2	780	0,0368
3000	21	776	0,037	21,2	776	0,0366
4000	21,2	780	0,0368	21,2	776	0,0366
5000	21,2	776	0,0366	21,2	772	0,0364
10000	21,2	766	0,0361	21,2	764	0,036
20000	21,2	748	0,0353	21,2	748	0,0353
30000	21	736	0,035	21	736	0,035
40000	21	724	0,0345	21	720	0,0343
50000	21	708	0,0337	21	712	0,0339
100000	20,8	572	0,0275	20,8	560	0,0269

B.2. First order low pass filter

B.2.1. Derivation of parameters

The transfer function of the first order low pass filter is determined by Equation B.1.

$$H(s) = \frac{\frac{R_2}{1+jwR_2C_2}}{R_1 + \frac{1}{jwC_1}} \tag{B.1}$$

This is determined by

$H(s) = \frac{V_{out}}{V_{in}} = -\frac{-Z_2}{Z_1} = \frac{\frac{R_2}{1+jwR_2C_2}}{R_1+\frac{1}{jwC_1}}$

$\frac{V_{out}}{Z_2} = -\frac{V_{in}}{Z_1}$

$Z_1 = R_1 + \frac{1}{jwC_1}$

$Z_2 = \frac{1}{\frac{1}{R_2}+jwC_2} = \frac{R_2}{1+jwR_2C_2}$

The capacitor C_1 can be neglected, it will not contribute to the transfer function, and a simplified version of the transfer function can be found in Equation B.2.

$$H_{simplified}(s) = \frac{R_2}{R_1(1 + jwR_2C_2)} \tag{B.2}$$

From Equation B.2 the DC gain K can be determined. The resistors R_1 and R_2 contribute to the DC gain. The gain K is equal to $K = H(0) = \frac{R_2}{R_1} = 0.15$.

In order to calculate the cut-off frequency the simplified transfer function, Equation B.2 will be used. The cut-off frequency can be derived in the following way:

$|H(jw)| = \frac{R_2}{R_1\sqrt{1+(wR_2C_2)^2}}$

$|H(jw_c)| = \frac{1}{\sqrt{2}}|H(0)|$

$\frac{R_2}{R_1\sqrt{1+(w_cR_2C_2)^2}} = \frac{1}{\sqrt{2}}\frac{R_2}{R_1}$

$1 + (w_c R_2 C_2)^2 = 2$
$w_c = \frac{1}{R_2 C_2}$
$f_C = \frac{1}{2\pi R_2 C_2}$

The cut-off frequency with the intended values is
$f_c = \frac{1}{2\pi R_2 C_2} = \frac{1}{2\pi 30 \cdot 10^3 \cdot 200 \cdot 10^{-12}} = 26525.8238486 = 26.5kHz$

The cut-off frequency with the real values is
$f_c = \frac{1}{2\pi R_2 C_2} = \frac{1}{2\pi 32 \cdot 10^3 \cdot 221 \cdot 10^{-12}} = 22504.9410481 = 22.5kHz$

B.2.2. Circuit

In Figure B.1 the circuit with the first order filter is shown. In Table B.3 the values of the components can be found. Error is calculated by Equation B.3

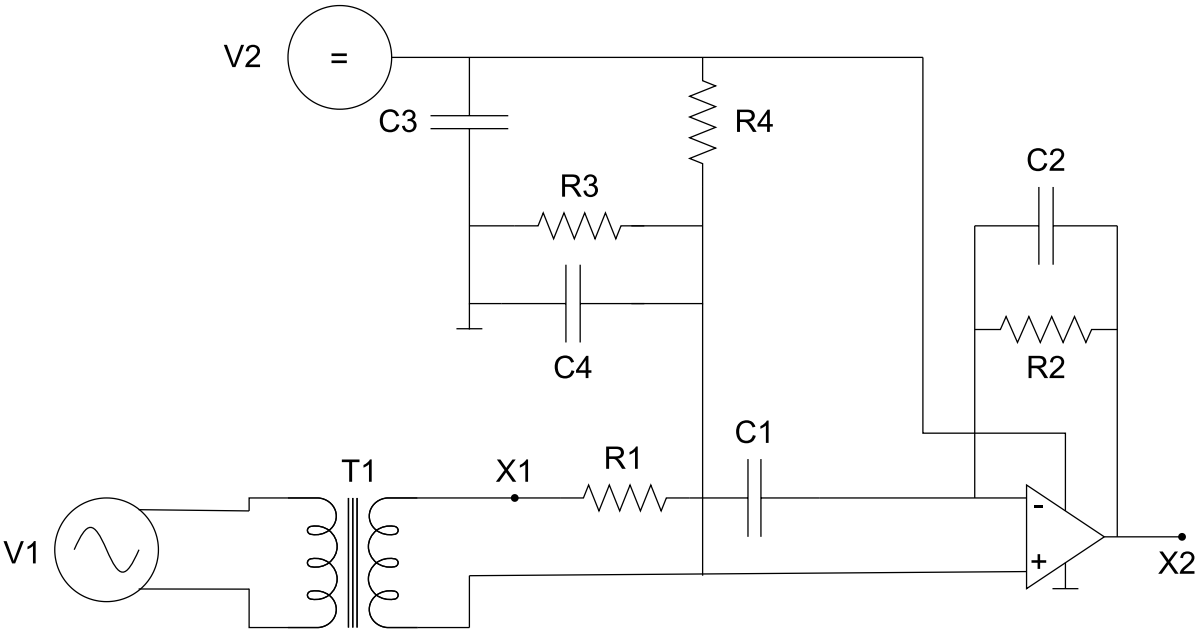

Figure B.1: Circuit with first order lowpass filter

$$Error = \frac{Realvalue - IntendedValue}{Intendedvalue} \cdot 100\% \tag{B.3}$$

Table B.3: Component values

Component	Intended value	Real value	Error [%]
R_1	200 kΩ	200 kΩ	0
R_2	30 kΩ	32 kΩ	6.67
R_3, R_4	150 Ω	148 Ω	-1.33
C_1	200 nF	235 nF	17.5
C_2	200 pF	221 pF	10.5
C_3	250 nF	321 nF	28.4
C_4	3 nF	3.13 nF	4.33

It is seen that the real used values vary a bit from the intended values that were used in LT-spice. The error for C_3 is the highest, 28.4%. It was hard to find the exact value for the components. This is just used for testing.

B.2.3. Setup for testing and Results

The setup for the testing was the following: at the input of the filter, point X_1 in Figure B.1, the function generator was connected. The input voltage was constantly set to 8.5 V, while the frequency was varied from 2 Hz till 100kHz. The output voltage, point X_2 in Figure B.1, was measured. The magnitude response was calculated by Equation 5.2.

$$M = \frac{V_{out}}{V_{in}} \tag{B.4}$$

Table B.4: Frequency response of first-order filter

Frequency [Hz]	Vin [V]	Vout [V]	Magnitude response
2	8,5	0,75	0,088
3	8,5	0,95	0,112
4	8,5	1,07	0,126
5	8,5	1,15	0,135
10	8,5	1,27	0,149
15	8,5	1,3	0,153
20	8,5	1,31	0,154
30	8,5	1,32	0,155
50	8,5	1,345	0,158
2300	8,5	1,33	0,156
6000	8,5	1,32	0,155
10000	8,5	1,24	0,146
20000	8,5	1,04	0,122
50000	8,5	0,56	0,066
100000	8,5	0,34	0,04

B.2.4. Low voltage tests

In Figure B.1 the circuit of the first order filter is shown. The output of the transformer X1 and Opamp X2 were tested. The function generator was set to different AC input voltages, ranging from 0.5 V till 10 V peak to peak at a constant frequency of 50 Hz. With the two channel digital storage oscilloscope the output values were measured. A picture of the setup can be found in Figure B.2

B.2.5. High voltage tests

In Figure B.3 the first implemented voltage sensing circuit for high voltage testing can be found. The voltage sensing module consists of:

- Two voltage sources: V_1 is the AC mains voltage and V_2 is the DC voltage of a power supply of 5V
- Switch device PC_1 is to provide safety for high voltage testing
- Transformer T_1 which scales down the voltage and decouples the AC
- A low pass filter, consisting of resistor R_2 and capacitor C_4, which filters the high frequency unwanted signals
- Resistors R_8, R_9 and capacitors C_5, C_6 which supply the operational amplifier O_1 with desired voltage and filter the high frequencies
- An operational amplifier O_1 which scales the voltage down to an useable value for Raspberry Pi

In Figure B.3 the output of transformer T_1 is denoted as X_1 and the output of the opamp O_1 is denoted as X_2.

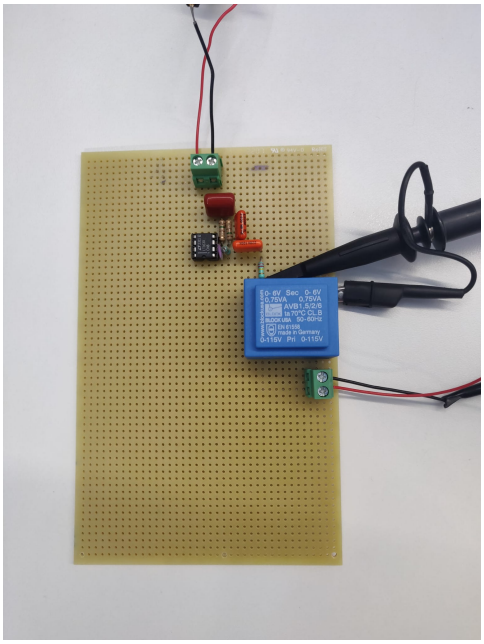

Figure B.2: Photo of voltage sensor test setup

B.3. Circuit with MFB filter

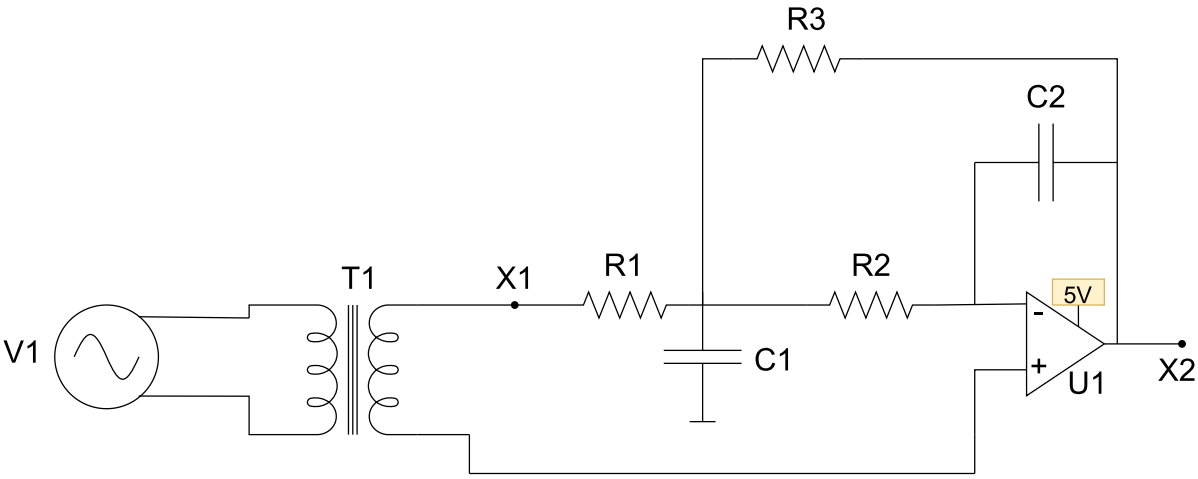

Figure B.3: Circuit with MFB filter

B.3.1. Low voltage test

The input V_{in} is a 20 V_{pk-pk} 50 Hz signal from the function generator.The input of the transformer and the output of the circuit, indicated as X2, is measured with the oscilloscope. This is a RMS voltage of $V_{RMS} = 7.07V$, which is calculated with Equation B.5

$$V_{RMS} = \frac{V_{pk-pk}}{2\sqrt{2}} \tag{B.5}$$

C

Current Transducer DC Testing

The current transducer DC testing was carried out using a $0 - 20V$, $5A$ programmable power supply and a 5Ω load capable of dissipating $300W$. The maximum possible current that can be delivered to the load using this setup is $4A$. The setup used to test the current transducer can be found in Figure C.1. The output of the current transducer is recorded using a multimeter. The input and output pins of the current transducer are connected according to the recommended pin setups, which can be found in Figure C.1, such that the number of primary turns is 1 and a primary resistance (R_p) of $0.24m\Omega$.

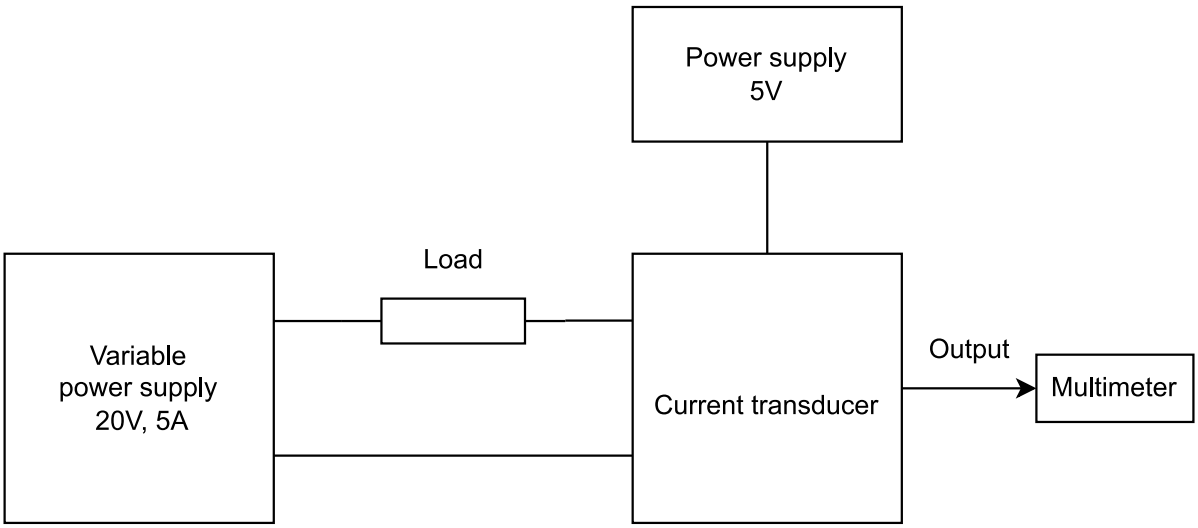

Figure C.1: Current transducer test setup

Table C.1: Examples of primary resistance according to number of primary turns (From CASR 15-NP datasheet [41])

Number of primary turns	Primary resistance R_P [mΩ]	Recommended connections
1	0.24	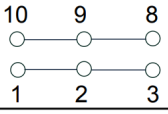
2	1.08	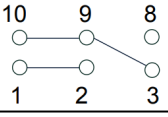
3	2.16	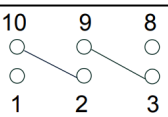

As mentioned previously, the theoretical sensitivity (G) of the current transducer is $41.67mV/A$. Equation C.1 is used to calculate the expected voltage at the output. An offset of voltage of 1.1 mV was present at the output of the current transducer before testing began. The error is then calculated using Equation C.2.

$$V_{expected} = G \cdot I_{in} + V_{offset} \tag{C.1}$$

$$Error = \frac{V_{measured} - V_{expected}}{V_{expected}} \cdot 100\% \tag{C.2}$$

The results the DC measurements of the current transducer can be found in Table C.2. It can be seen that $V_{measured}$ and $V_{expected}$ are almost the same, they vary by a very small percentage. The error is very small, always under the 0.3%. It might be possible that the error is due to the accuracy of the multimeter. It was seen during the testing that the input current which was intended to be supplied, and the current that was really supplied varied a little. The supplied current was a little less than the intended current. They differed starting at 1.25 A, with a difference of 0.2 mA. This increased a little until 3.75 A, where the difference was: 0.9 mA. This might also cause this error.

Table C.2: Current transducer DC measurement

Iin [A]	Difference [mA]	Expected Vout [mV]	Measured Vout [mV]	Error [%]
0,25	0	11,5	11,5	-0,15
0,5	0	21,9	22	0,3
0,75	0	32,4	32,4	0,15
1	0	42,8	42,9	0,3
1,25	0,2	53,2	53,3	0,21
1,5	0,3	63,6	63,8	0,31
1,75	0,4	74	74,2	0,24
2	0,4	84,4	84,6	0,19
2,25	0,5	94,9	95,1	0,26
2,5	0,6	105,3	105,5	0,21
2,75	0,7	115,7	116	0,27
3	0,8	126,1	126,4	0,23
3,25	0,8	136,5	136,9	0,27
3,5	0,8	146,9	147,3	0,24
3,75	0,9	157,4	157,7	0,21

D

Current Sensor

D.1. High-Current Sensor Measurement Setup

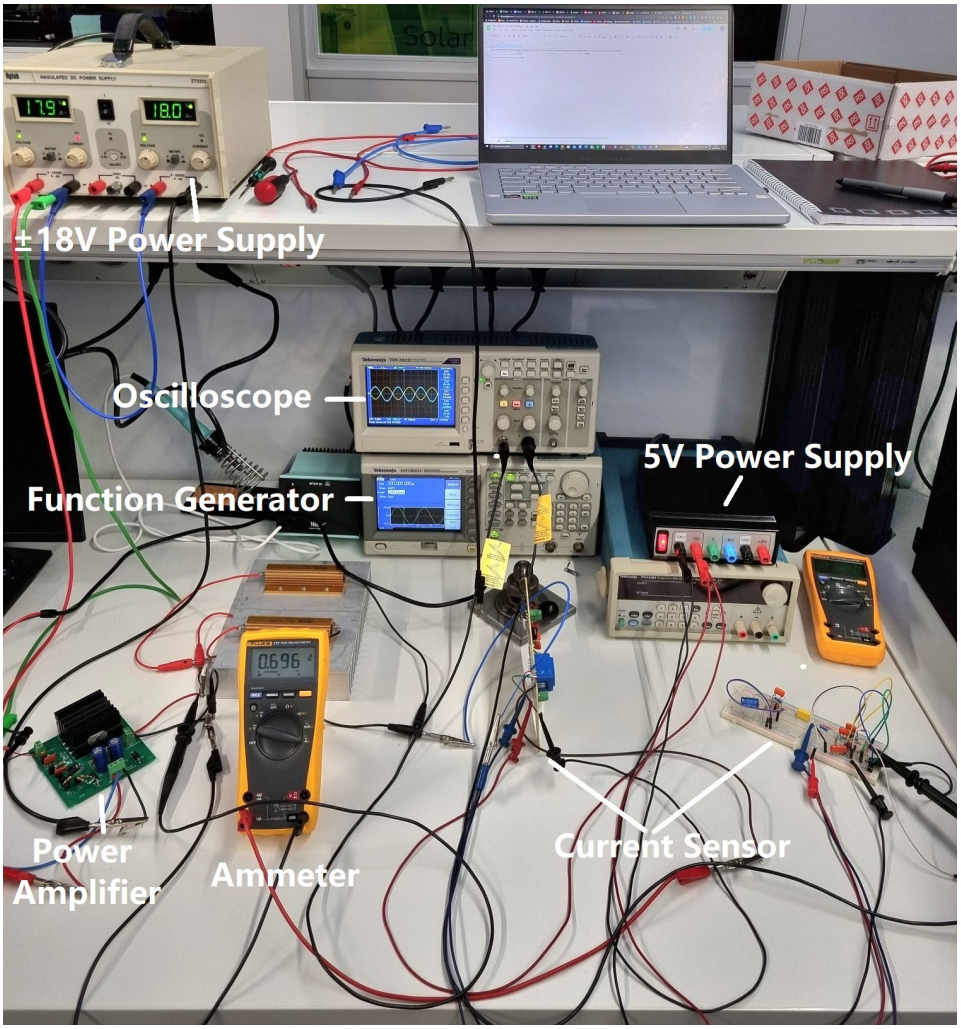

Figure D.1: Annotated photo of measurement setup used to test low-current sensor

D.2. High-Current Sensor Measurement Setup

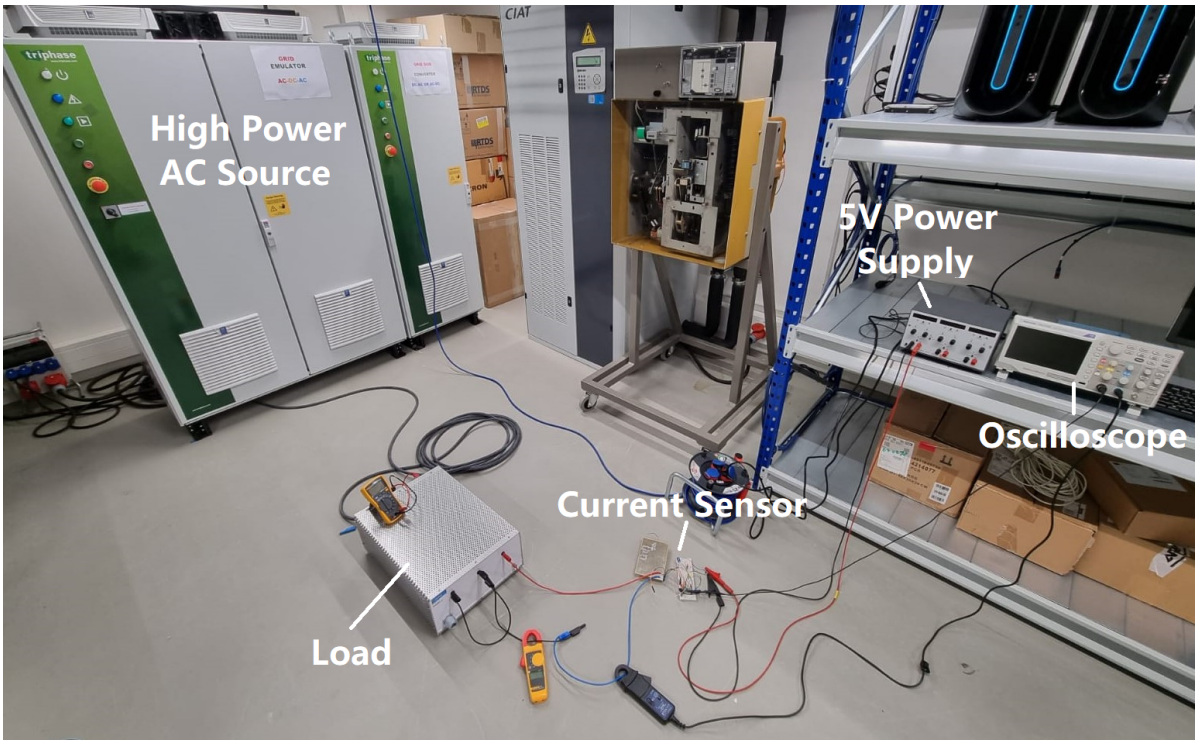

Figure D.2: Annotated photo of measurement setup used to test high-current sensor

D.3. Low-Current Sensor Measurement Setup

The power supply of the signal amplifier provides a DC voltage of ± 18 and a maximum current of 2A. The signal amplifier amplifies the signal 25 times. This amplified signal is the input of the PCB. In the PCB, the signal goes through the current sensing module, the output voltage is measured. The load that is used are

The results can be found in Table D.1.

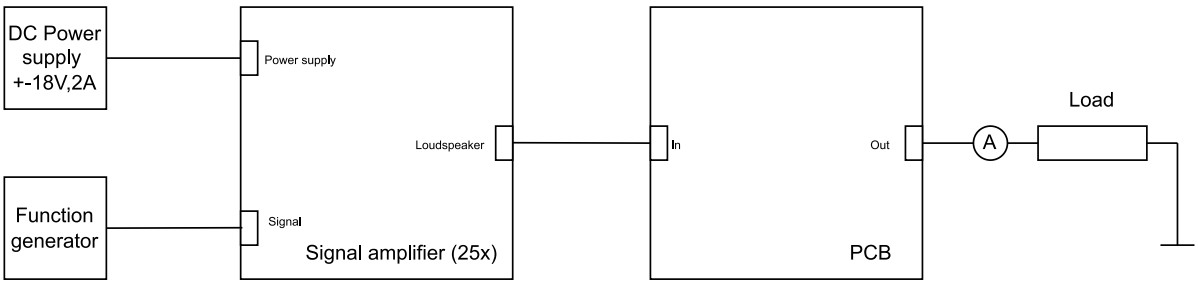

Figure D.3: Current sensing setup

Ch1 is the output of the power amplifier in rms voltage. To calculate the expected rms voltage of ch1, Equation D.1 could be applied. In order to calculate the expected current that is the input of the current transducer Equation D.2, is applied, the load that is used is 5Ω. Ch2 is the output of the current sensor. In order to calculate the expected output of the current sensor, Equation D.3 is applied, where the sensitivity of the transducer G is 41.67mV/A, the gain of MFB filter is 21.36 and the voltage $V_{RaspberryPi}$ is 3.3V, and V_{max} is 5V.

$$V_{rms,expected,ch1} = \frac{V_{pk-pk,in}}{2\sqrt{2}} \cdot 50 \tag{D.1}$$

$$I_{rms,expected} = \frac{V_{rms,expected,ch1}}{Load} \tag{D.2}$$

$$V_{rms,expected,ch2} = I_{rms,expected} \cdot G_{transducer} \cdot G_{MFB} \cdot \frac{V_{RaspberryPi}}{V_{max}} \tag{D.3}$$

Table D.1: Low current sensing PCB output

Test	Signal Generator input V_{pk-pk} [mV]	Ch1: V_{RMS} measured [V]	Ch1: V_{RMS} expected [V]	Error Ch1 [%]	Measured I_{RMS} [A]	Expected I_{RMS} [A]	Error current [%]	Ch2: V_{RMS} measured [V]	Ch2: V_{RMS} expected [V]	Error Ch2 [%]
1	100	1.78	1.77	0.69	0.334	0.354	5.53	0.197	0.208	5.15
2	150	2.67	2.65	0.69	0.5	0.53	5.72	0.295	0.312	5.31
3	200	3.56	3.54	0.69	0.666	0.707	5.81	0.392	0.415	5.63
4	250	4.44	4.42	0.47	0.831	0.884	5.98	0.488	0.519	6.02
5	300	5.35	5.3	0.88	0.996	1.061	6.1	0.594	0.623	4.67
6	350	6.24	6.19	0.85	1.16	1.237	6.26	0.692	0.727	4.8
7	400	7.13	7.07	0.83	1.33	1.414	5.95	0.793	0.831	4.55
8	450	8.03	7.95	0.94	1.499	1.591	5.78	0.893	0.935	4.45
9	500	9.81	8.84	10.99	1.667	1.768	5.7	0.993	1.038	4.38
10	550	9.79	9.72	0.69	1.843	1.945	5.22	1.1	1.142	3.7
11	600	10.7	10.61	0.88	2.008	2.121	5.34	1.18	1.246	5.31

E

First order filter

During simulation of the voltage transformer a small DC current through the secondary coil was detected, this was unwanted behaviour because it would also offset the output of the filter and thus change the range for the ADC. Another important effect is DC currents will saturate the transformer core, introducing Voltage harmonics and hysteresis.[48, 49] However this could be resolved by either placing a capacitor between the transformer and input of the circuit or by making the input impedance of the larger. Using the simulations a pole was found formed by the feedback resistors and the total capacitance at the inverting input, a few solutions to get this pole to be stable were given:

- lower the value of the resistors
- add a feedback capacitor of 10pF or more

It was decided to add the capacitor C_2 with an intended capacitance of 200 pF, the real value was 221 pF.

E.1. Filter testing

The first order filter, as explained in subsection 5.3.1, was tested. The first order filter circuit can be found in Figure B.1, the setup and the results can be found in subsection B.2.3. The final frequency response of this filter can be found in Figure E.1. Due to component tolerances, the real world values varied slightly from the ideal values. The filter was tested using a function generator on the input and an oscilloscope attached to the output.

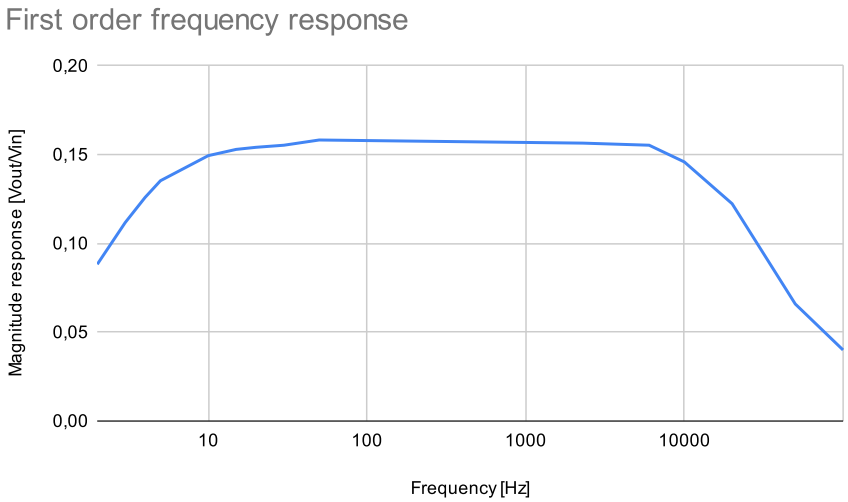

Figure E.1: Frequency response of first order filter and transformer

The magnitude response from 20 Hz to 6 kHz is consistent, around 0.158, this magnitude response was as was expected with a gain of 0.15. The lower frequencies up to 10 Hz and the higher frequencies from 10 kHz result in a lower magnitude response. The variations in the frequency response between 10 Hz and 10 kHz are relatively small, therefore Requirement 3.3 is fulfilled. Comparing this to the datasheet [32], the magnitude response should have been consistent over a bandwidth of 100 Hz till 300 kHz. It is unclear why at a higher frequency than 20 kHz, the magnitude response decreases. It is not a problem that the expected value deviates from the real value. It is aimed to use the op amp at 50 Hz. It can be concluded that the op amp works well for the intended setup.

The low voltage tests for the first order filter have been done on circuit board. The setup can be found in subsection B.2.4. The results can be found in Table E.1. The expected output of transformer X1 was calculated by Equation E.1. The magnitude response at 50 Hz, 0.039, was used. The expected output of op amp X2 was calculated by Equation E.2, using the gain 0.15 of the filter.

Table E.1: Output of transformer and op amp under low voltage test values

Input Vpk-pk [V]	Measured Output X1 Vpk-pk [mV]	Expected output X1 Vpk-pk [mV]	Error X1 [%]	Measured output X2 Vpk-pk [mV]	Expected output X2 Vpk-pk [mV]	Error X2 [%]
0,5	20	19.5	2.6	4,5	3	50
1	39	39	0	6,75	5,85	15,4
2	77	78	1.3	12,5	11,55	8,2
5	190	195	2.6	29,2	28,5	2,5
10	380	390	2.6	57,5	57	0,9

$$X1_{expected} = Input \cdot M_{X1,50Hz} = Input \cdot 0.039 \tag{E.1}$$

$$X2_{expected} = X1_{measured} \cdot Gain = X1_{measured} \cdot 0.15 \tag{E.2}$$

The next test was to test the first order filter circuit on high voltages. The setup is similar to the setup of the low voltage tests in Figure B.1. The voltage RMS and pk-pk is both measured. In Table E.2 the results and expected values can be found. Expected outputs X1 and X2 can be calculated by the same equations that were used for the voltage tests: Equation E.1 and Equation E.2. The results show that the errors are really small, therefore it can be concluded that voltage sensing works very well for high voltages.

Table E.2: High voltage measurements first order filter

	Measured Output X1	Expected Output X1	Error [%]	Measured Output X2	Expected Output X2	Error [%]
Vpk-pk [V]	24,8	25,4	-2,3	3,76	3,72	1,1
Vrms [V]	8,84	8,97	-1,4	1,33	1,326	0,3

F

Matlab power spectral density plot

```
close all
x=DATA(:,2);
y = pspectrum(x);
n = 4096;%length(x);          % number of samples
fs = 50000;
f = (0:n-1)*(fs/(2*n));     % frequency range
%power = abs(y).^2/n;    % power of the DFT

loglog(f,y,'LineWidth',1.5)
grid on;
xlabel('Frequency [Hz]');
ylabel('Power');
xlim([10 10000]);
xline([50 250 350 950 1450], 'LineWidth',1.5);
plim= interp1(f,y,50);
yline(plim*.0005^2);
interp1(f,y,250);
interp1(f,y,350);
interp1(f,y,950);
interp1(f,y,1450);

hold on;
plot(50,interp1(f,y,50),'o', 'LineWidth',4, 'Color','r');
plot(250,interp1(f,y,250),'o-', 'LineWidth',4, 'Color','r');
plot(350,interp1(f,y,350),'o-', 'LineWidth',4, 'Color','r');
plot(950,interp1(f,y,950),'o-', 'LineWidth',4, 'Color','r');
plot(1450,interp1(f,y,1450),'o-', 'LineWidth',4, 'Color','r');
```

G

Prototype Photos

Figure G.1: Photo of the outside of the Prototype

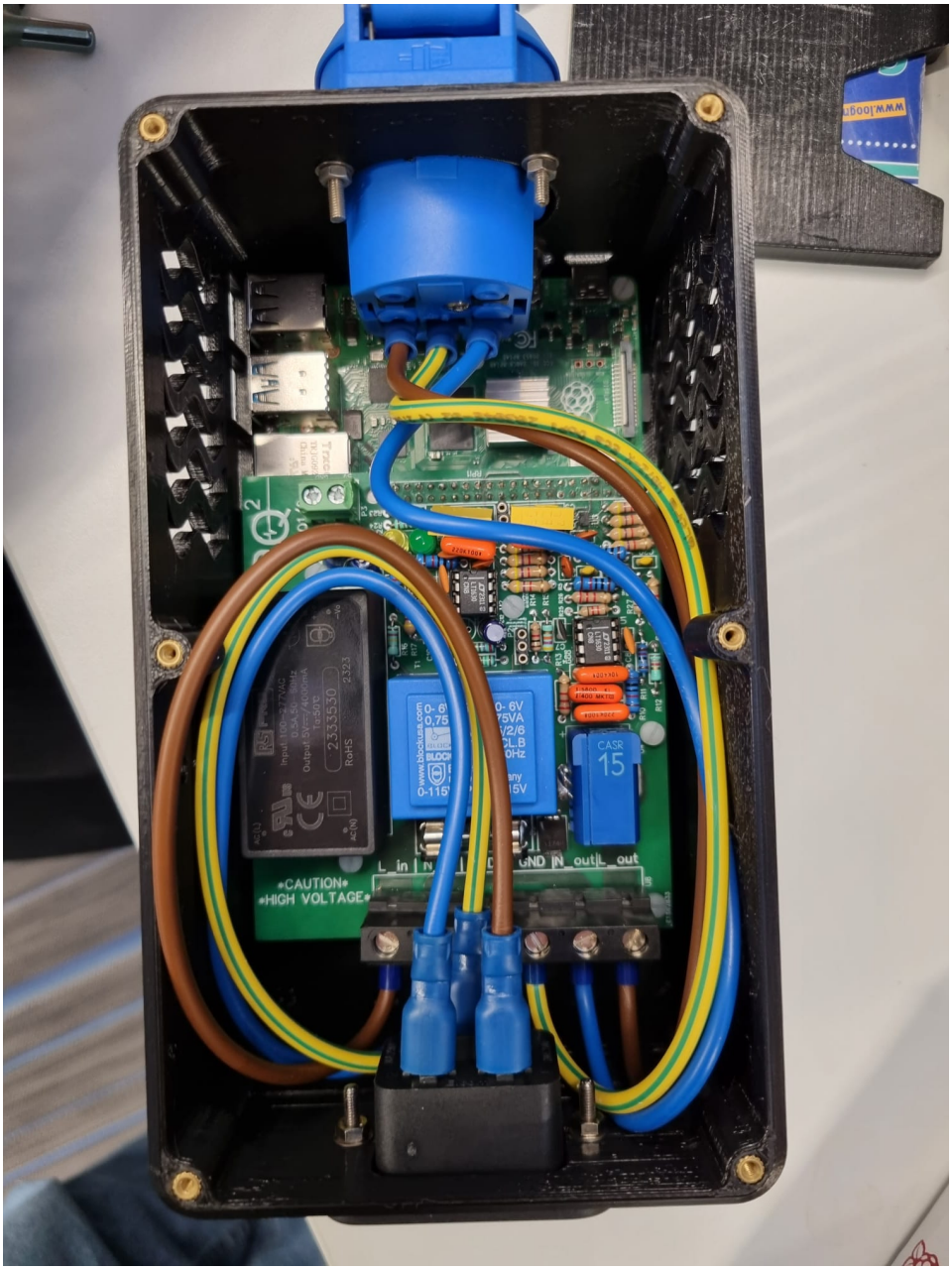

Figure G.2: Photo of the inside of the Prototype

H

Protection

Schematic of circuit breaker made by Remko Koornneef indicated in Figure H.1.

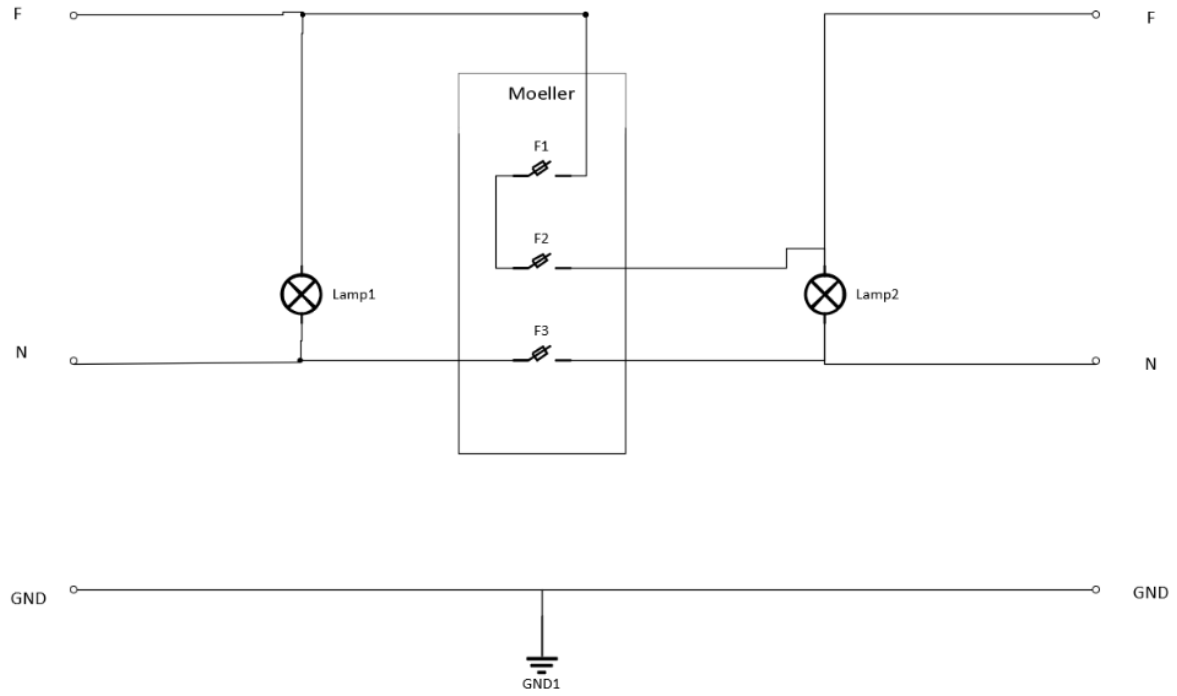

Figure H.1: Circuit breaker for protection

I

PCB

I.1. PCB Test Results no load

The input V_{RMS} was measured with a multimeter. The input I_{RMS} was measured with a current clamp. The resistor box of 3 x 2.2Ω is connected. The properties of this resistor box is that it has a power of 1500 W and a maximum current of 20A.

The output of channel 1(yellow) is the voltage sensor ouput in RMS mV. The output of channel 2 (blue) is the current sensor output in RMS mV. The outputs are measured with an oscilloscope. The setup can be found in Figure I.1

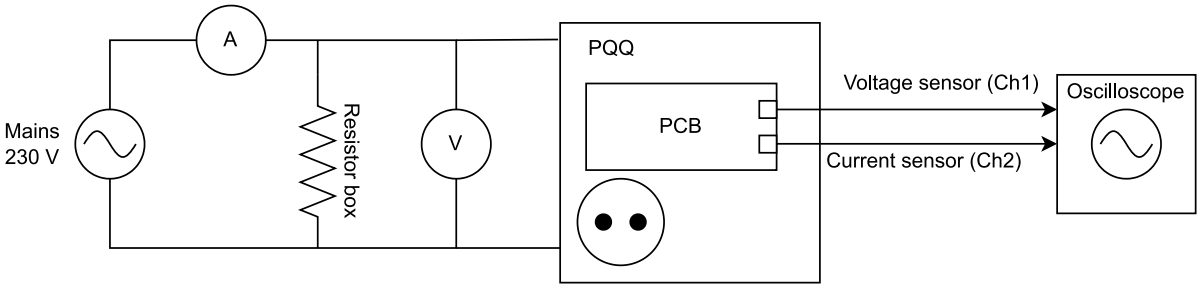

Figure I.1: Setup for testing no load

The measured values of ch1 and 2 were measured with a probe with attenuation of 10. Therefore, for the real value of the channels, it should be multiplied by 10. The expected output of the voltage sensor ch1 can be calculated with Equation I.1. V_{RMS} is the input voltage measured with a multimeter.

Table I.1: No load measurements all channel measurements done in RMS voltage

Picture	Description	Input Vrms [V]	Input Irms [A]	Measured Ch1 [mV]	Real Ch1 [mV]	Expected Ch1 [mV]	Error Ch1 [%]	Measured Ch2 [mV]	Real Ch2 [mV]	Expected Ch2 [mV]	Error Ch2 [%]
13	No load	233,6		74,2	742	759,2	-2,3	2,09	20,9	\	
14	No load	233,5		74	740	758,8	-2,5	2,08	20,8	\	

The graphs of the two tests can be found in Figure I.2, Figure I.3

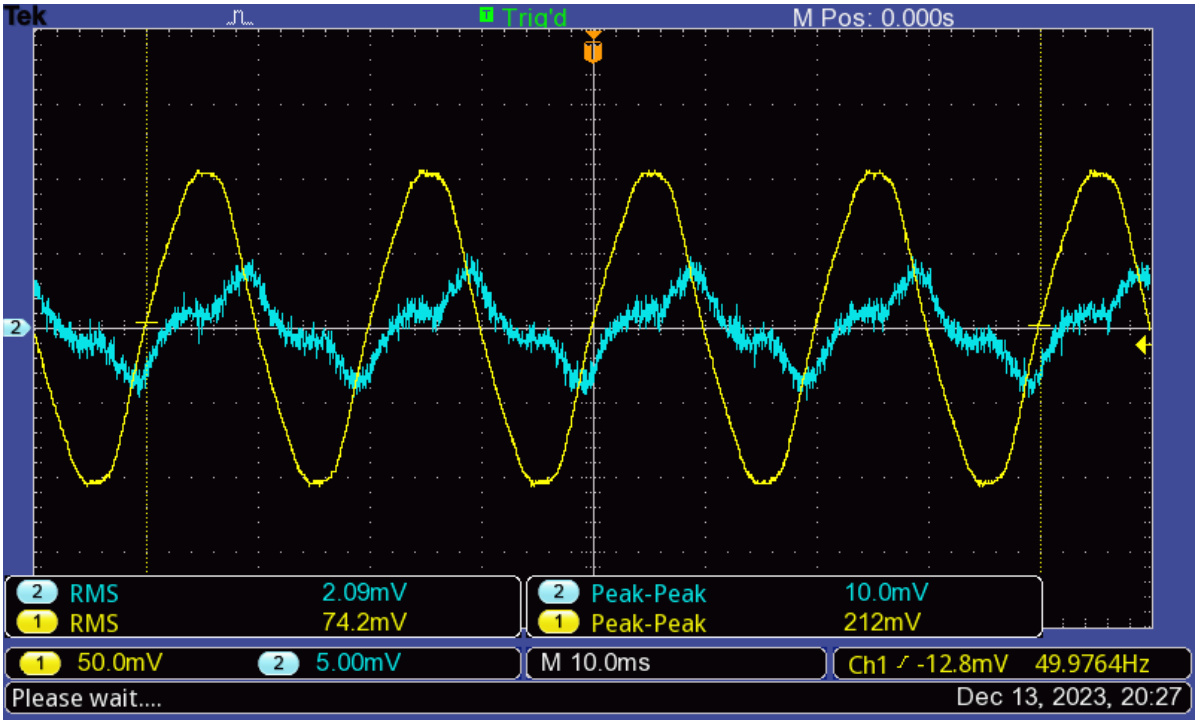

Figure I.2: Test 13

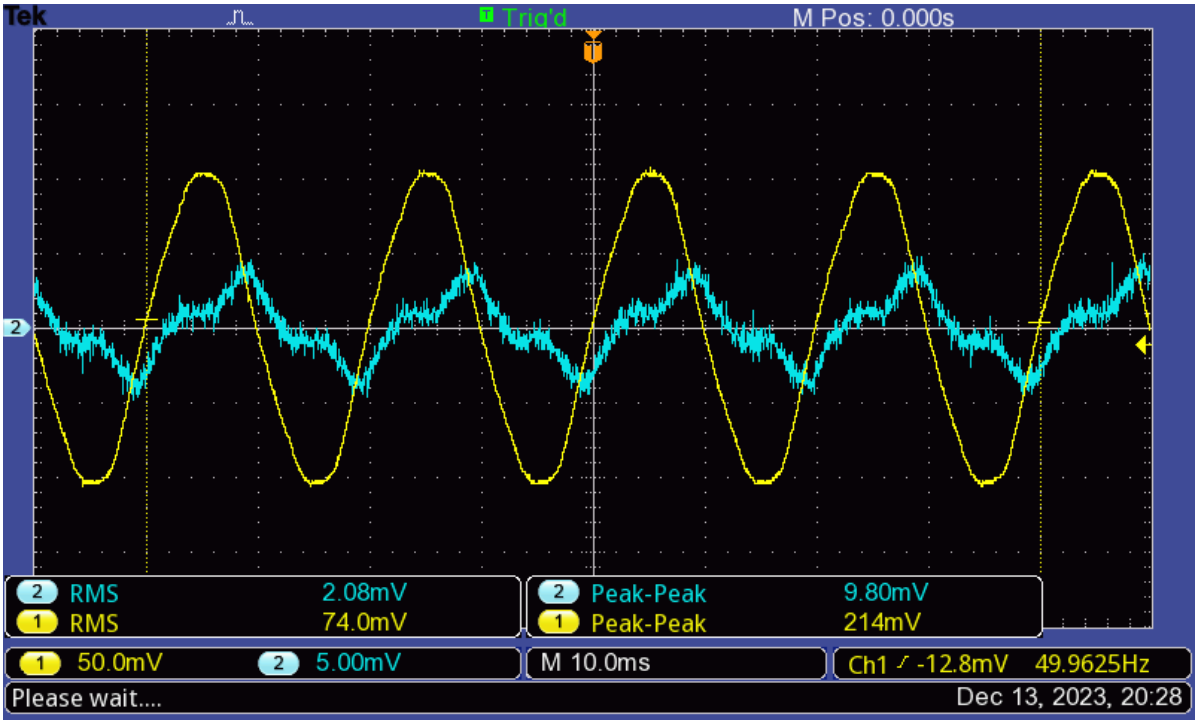

Figure I.3: Test 14

I.2. PCB Test Results on Hot Plate

The input V_{RMS} was measured with a multimeter. The input I_{RMS} was measured with a current clamp. The product PQQ is connected. Via the plug a device can be connected to PQQ. The device that is connected is a hotplate of 2500W, Tomado HVLnr78.05 The output of channel 1(yellow) is the voltage

sensor ouput in RMS mV. The output of channel 2 (blue) is the current sensor output in RMS mV. The outputs are measured with an oscilloscope. The setup can be found in Figure I.4

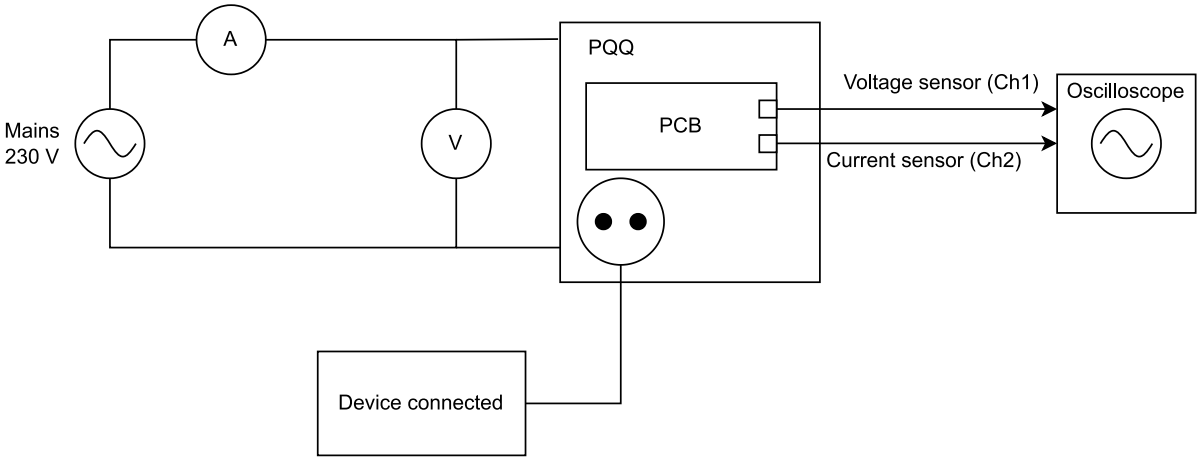

Figure I.4: Setup PCB high voltage, current tests with load

The measurements can be found in Table I.2 The measured values of ch1 and 2 were measured with a probe with attenuation of 10. Therefore, for the real value of the channels, it should be multiplied by 10. The expected output of the voltage sensor ch1 can be calculated with Equation I.1. V_{RMS} is the input voltage measured with a multimeter. M_{x1} is the magnitude response of the transformer: 0,039. G_{MFB} is the gain of the MFB filter: 0,0833. To get the output in mV it is divided by a factor of 1000. The expected output of the current sensor ch2 can be calculated with Equation I.2. I_{RMS} is the input current measured with a current clamp. $G_{transducer}$ is the gain of the transducer: 41,67 $\frac{mV}{A}$. G_{MFB} is the gain of the MFB filter. The gain of the MFB filter depends on the current signal; for low currents, it is 21.36, whereas for high currents, it is 1.8. During measurements with the cooker, currents of 4.4A, 6.4A, and 10A were drawn. Since the low current sensor is effective up to 2A, and more current was drawn, the high current sensor with a gain of 1.8 is used for the calculations. $V_{Raspberrypi}$ is the voltage of the Raspberry Pi of 3.3V, V_{max} is the maximum voltage of 5V

$$Ch1_{expected} = \frac{V_{RMS}}{1000} \cdot M_{x1} \cdot G_{MFB} \tag{I.1}$$

$$Ch2_{expected} = I_{RMS} \cdot G_{transducer} \cdot G_{MFB} \cdot \frac{V_{Raspberrypi}}{V_{max}} \tag{I.2}$$

Table I.2: Measurements on various loads, all channel measurements done in RMS voltage

Figure	Description	Input Vrms [V]	Input Irms [A]	Measured Ch1 [mV]	Real Ch1 [mV]	Expected Ch1 [mV]	Error Ch1 [%]	Measured Ch2 [mV]	Real Ch2 [mV]	Expected Ch2 [mV]	Error Ch2 [%]
15	Hot plate (low)	232,9	4,4	73,3	733	756,9	-3,2	21,1	211	217,8	-3,1
16	Hot plate (medium)	232,8	6,4	73	730	756,6	-3,5	30,7	307	316,8	-3,1
17	Hot plate (high)	231,5	10	72,2	722	752,4	-4	51,3	513	495,0	3,6

The pictures of the graphs of the hotplate for various settings are shown in Figure I.5,Figure I.6 and Figure I.7

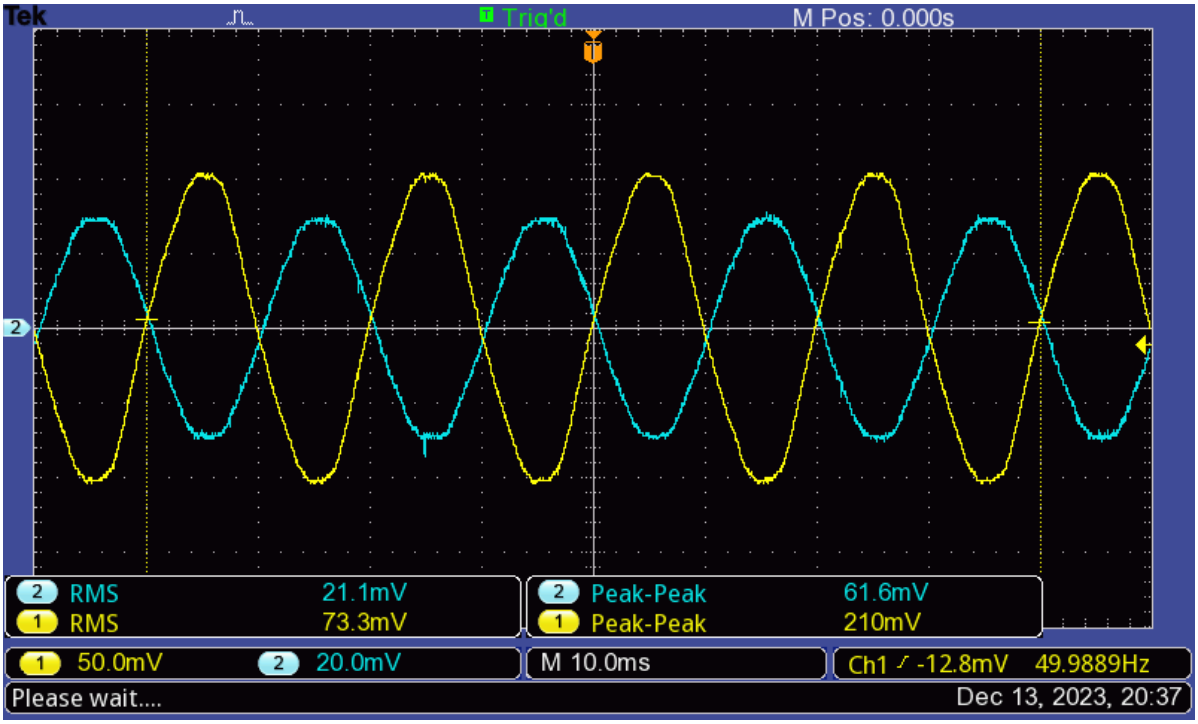

Figure I.5: Test 15: Small hotplate consuming $4.4A_{RMS}$ at $232.9V_{RMS}$, CH1 (Yellow) Output of voltage sensor, CH2 (Blue) Output of high current sensor

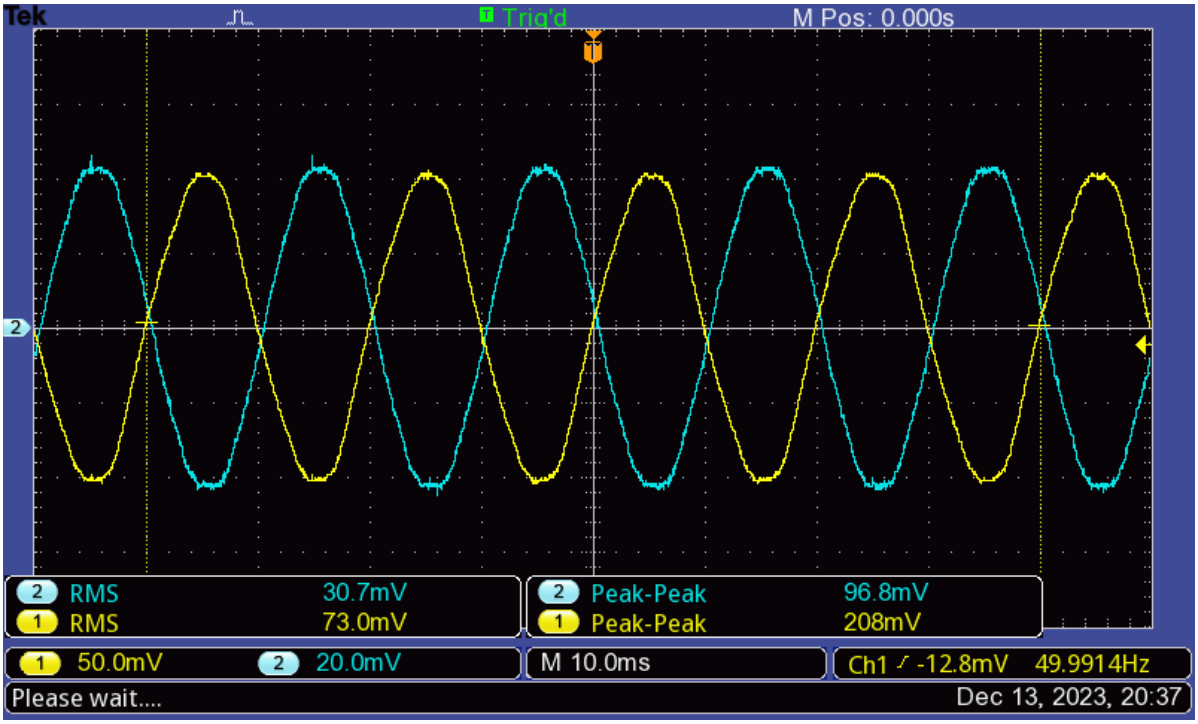

Figure I.6: Test 16: Larger hotplate consuming $6.4A_{RMS}$ at $232.8V_{RMS}$, CH1 (Yellow) Output of voltage sensor, CH2 (Blue) Output of high current sensor

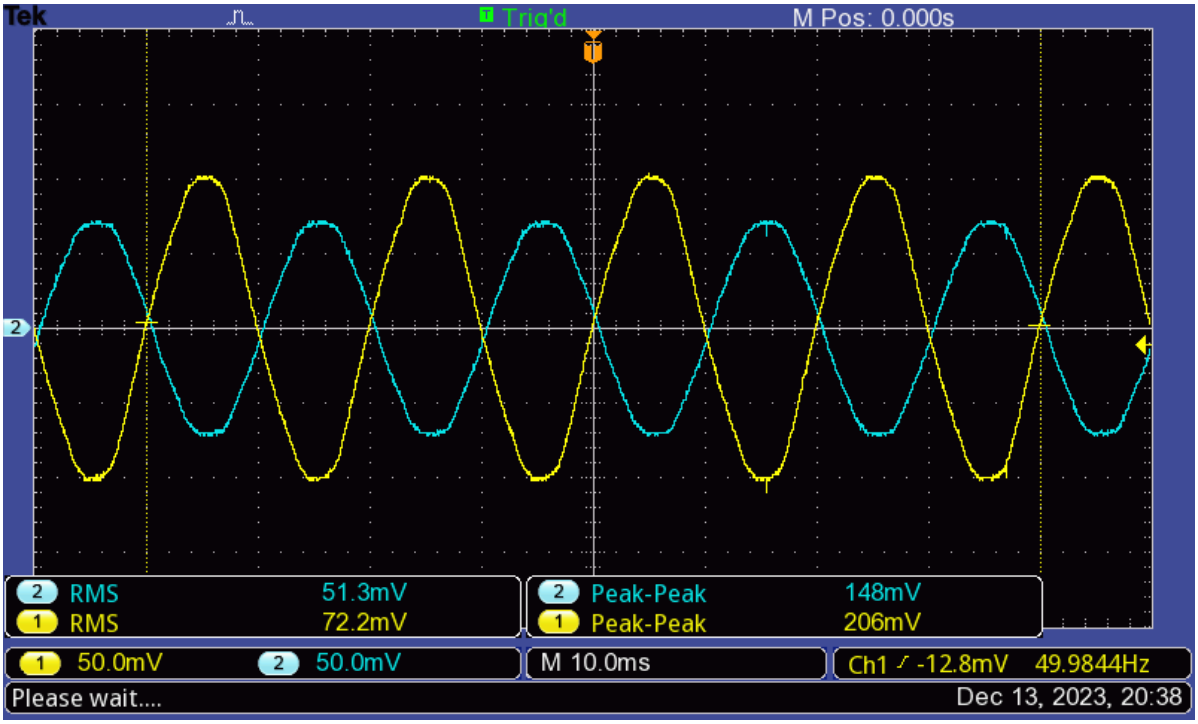

Figure I.7: Test 17: Both plates powered simultaneously consuming $10A_{RMS}$ at $231.5V_{RMS}$, CH1 (Yellow) Output of voltage sensor, CH2 (Blue) Output of high current sensor

I.3. PCB test results of harmonics

The setup for testing the harmonics is given in Figure I.8. The voltage source was a generated 220V for 1-phase. The voltage was measured with a multimeter, the current was measured with a current clamp. The resistor box that was connected was 3 x 100Ω, 2500W, 4,8A max.

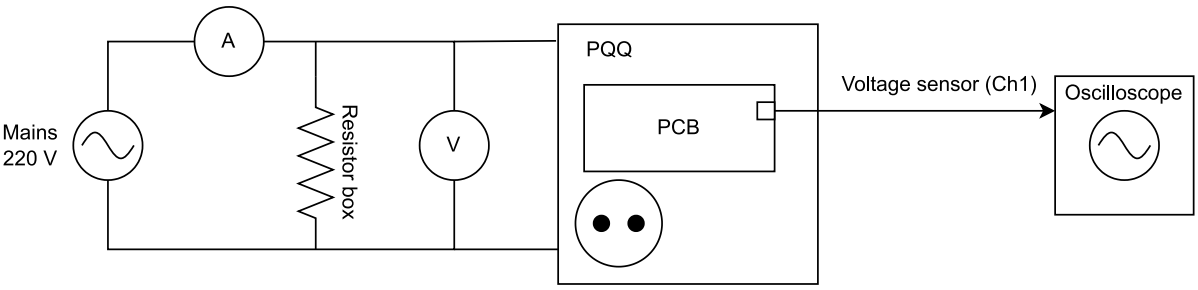

Figure I.8: Setup for testing harmonics

The voltage was measured with a multimeter, it resulted in 382,7 V. To obtain the single-phase value, Equation I.3 is applied, and that results in 220,95 V. The current was measured with a current clamp. The output of channel 1, voltage sensor, was measured with a probe with an attenuation of 10 and was connected to an oscilloscope. Therefore, to get the real output value the measured output should be multiplied with a factor of 10. See Table I.3 for the measured values. The graphs of the measurements can be found in Figure I.9

$$V_{\phi} = \frac{V_{3\phi}}{\sqrt{3}} \tag{I.3}$$

Table I.3: Measured values of harmonics

Measured Vrms [V]	Input Vrms [V]	Irms [A]	Measured Ch1: Vrms [mV]	Real Ch1: Vrms [mV]	Expected Ch1: Vrms [mV]	Error Ch1 [%]
382,7	220,95	2,2	70,4-70,9	704-709	718	1,3-1,9

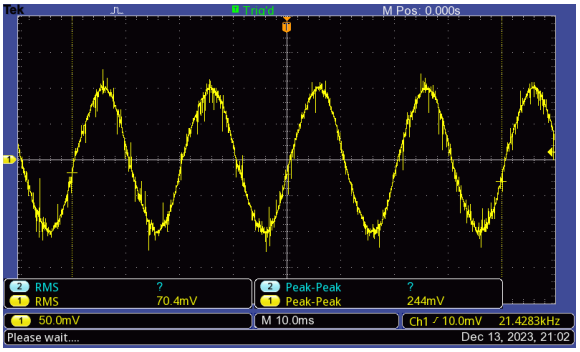

(a) Test 1

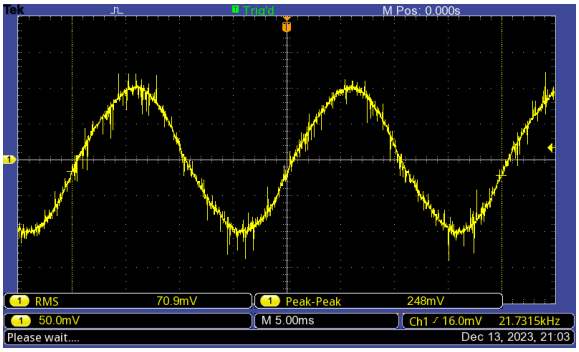

(b) Test 2

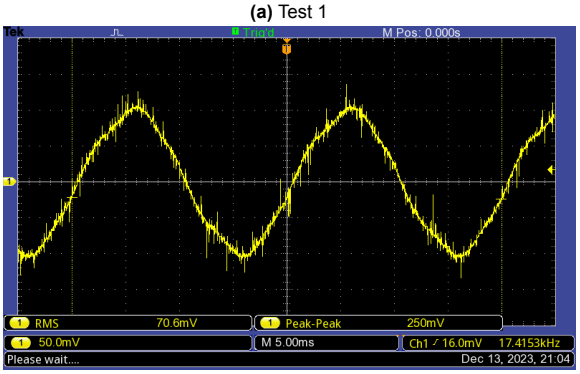

(c) Test 3

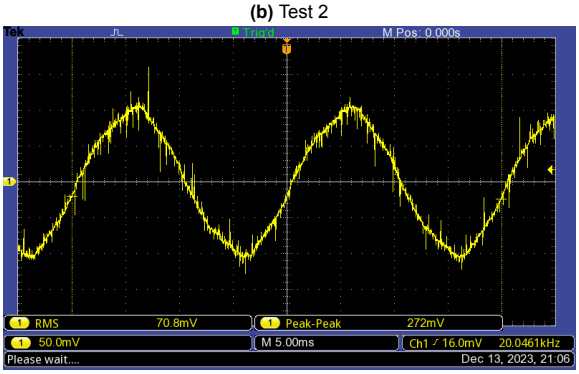

(d) Test 4

Figure I.9: Harmonic test

I.3.1. PCB

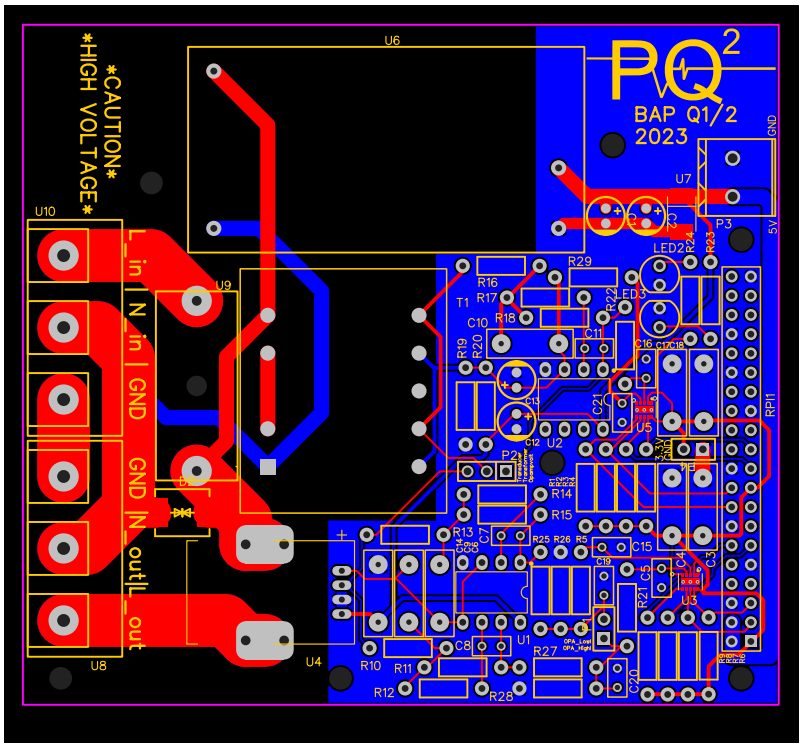

Figure I.10: PCB

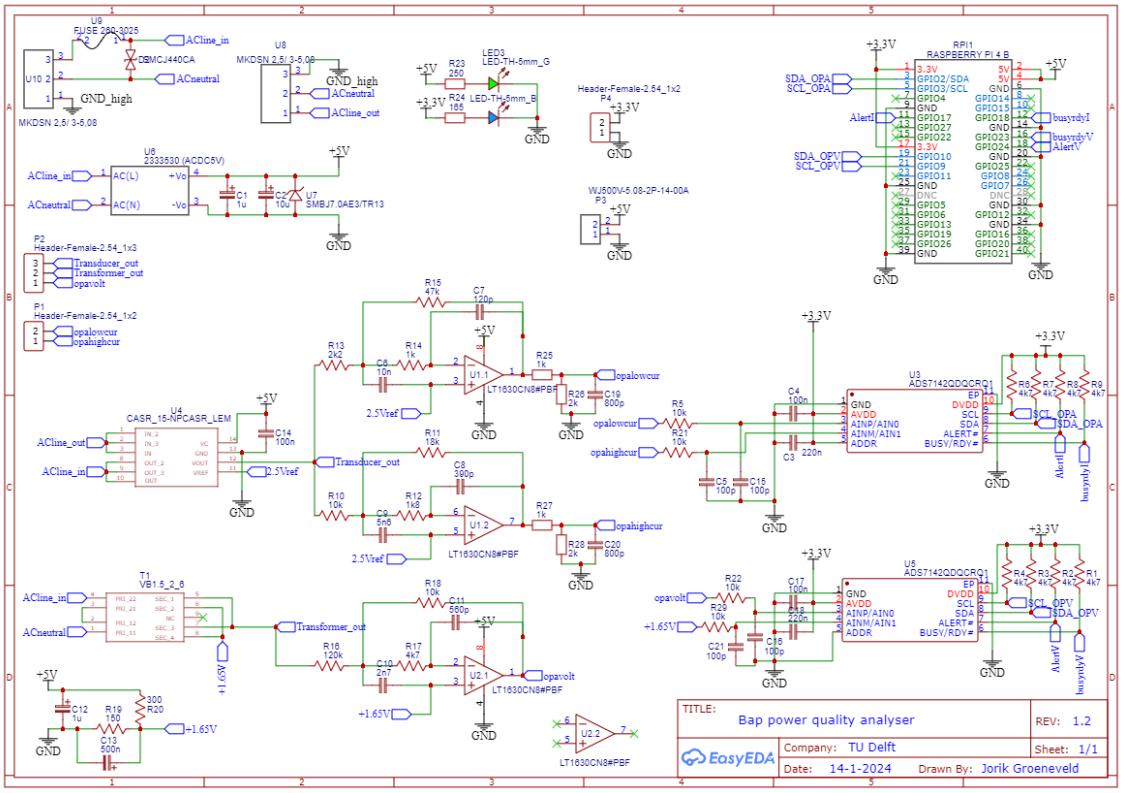

Figure I.11: Caption

J

Quality factor

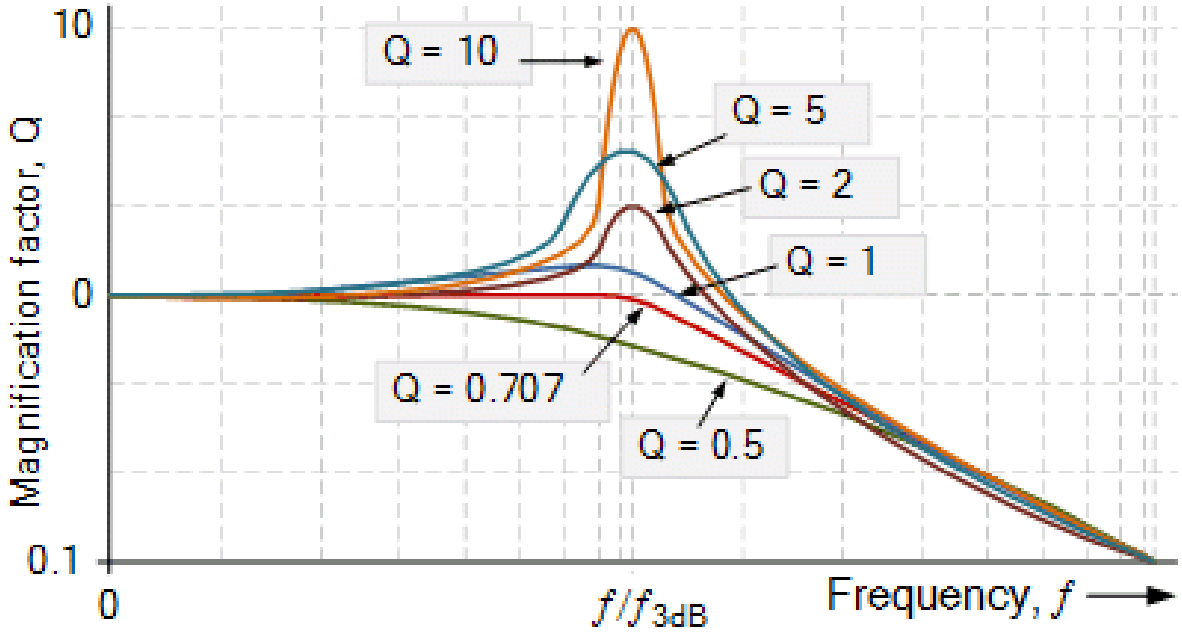

Figure J.1: Different quality factors show different peaking behaviour.[53]

K

Assembly Costs

Table K.1: Table containing the costs of all components required to produce the prototype

Component	Quantity	Cost per Unit (€)	Total Costs (€)
BLOCK VB1.5/2/6 (Voltage Transformer)	1	10.98	10.98
5V DC Power Supply	1	12.97	12.97
CASR 15-NP (Current Transducer)	1	17.40	17.40
AD7142-Q1 (ADC)	2	2.69	5.38
LT1630 (Op amp)	2	8.13	16.26
Plug Socket, 16A, Type F	1	5.70	5.70
IEC Connector Male, 20A, 250V	1	1.54	1.54
IEC C19 Socket Power Cable	1	14.52	14.52
PCB (Including shipping costs)	1	5.184	5.184
SMBJ7.0A (TVS Diode Power Supply)	1	0.40	0.40
SMCJ440CA (TVS Line Diode)	1	0.856	0.856
3D Printed Enclosure	1	37.27	37.27
Raspberry Pi Pin Extender	1	1.87	1.87
Raspberry Pi 4B 4GB	1	61.95	61.95
Micro SD card (128 GB)	1	13.29	13.29
Raspberry Pi Heat sink	1	1.30	1.30
Fuse Mount (65600001009)	1	1.51	1.51
16A Fuse	1	0.791	0.791
Cable Contact Points (ESPM03200)	2	2.17	4.34
Lid screws (50M025045P020)	6	0.121	0.726
Screw Mounts (IUTB-M2.5)	15	0.27	4.05
Mounting Screws (50M025045F006)	9	0.121	1.089
Misc (Resistors, Cable, etc)	1	5.00	5.00
Total Costs to Assemble Entire Unit			224.38